5. Introduction

Neuropathic pain (NP) is a critical and complex illness often occurring from injury to the somatosensory nervous system that eventually results in the development of multiple enduring and intricate pain syndromes (Colloca, Ludman et al. 2017). The assortment of symptoms commonly observed clinically may occur spontaneously or triggered, resulting in an increased sensitivity to pain (hyperalgesia) along with the perception of painful burning, stabbing, or electric shock-like sensations (Bannister, Sachau et al. 2020). Reportedly, the complex neuropathological mechanisms that underlie the development of NP involve sensory nociceptors and spinothalamic tract sensitization, resulting in peripheral and central sensitization (Meacham, Shepherd et al. 2017). Further, dysregulation of ion channels is reported to enhance the primary afferent neuron excitability, causing ectopic action potentials in the peripheral nervous system (PNS) (Baron 2006). All these events cause secondary neuroplastic changes in the spinal cord (SC) and brain multi-receptive neurons along with dampening the descending inhibitory pathways (Woolf and Mannion 1999). Currently, the therapeutic first-line strategies for managing chronic NP clinically include calcium channel blockers (CCBs) such as pregabalin and gabapentin (Tong, Zhengyao et al. 2021). However, its effectiveness is hindered as the pathophysiology of NP is complex involving overlaying of ion channel modulation with neuroimmune interactions (Vicario, Turnaturi et al. 2020). Besides, there is also a lack of comprehensive knowledge on the temporal changes in the ionic concentration post-injury. Therefore, there is a need to monitor the time-dependent changes in the calcium concentration $(Ca^{2+})_i$ in NP in order to identify the optimal timeframe for initiating pharmacological intervention as the time of treatment commencement is important for better efficacy.

Dysregulation of calcium homeostasis following neuronal injury is a crucial factor that contributes to the development and maintenance of NP (Siau and Bennett 2006, Cui, Wu et al. 2021). Studies have reported alteration in the voltage-gated calcium channel (VGCC) expression, leading to an elevation in the inflow of Ca^{2+}, which in turn mediates a variety of neuronal processes, including membrane excitability, neurotransmitter release, synaptic plasticity along with the release of pro-inflammatory cytokines, resulting in an exacerbation of pain sensation following sciatic nerve (SN) damage (Berridge, Lipp et al. 2000, Yaksh 2006). Similarly, the SC also exhibit enhanced $(Ca^{2+})_i$ due to upregulation in the VGCC activity in various animal models of NP (Kawamata and Omote 1996, Tilley, Cedeño et al. 2022). In addition, the activation of calcium-permeable receptors, such as TRPV1, leads to an increase in $(Ca^{2+})_i$ levels, which in turn promotes neuronal hyperexcitability (Liu, Miao et al. 2023). These mechanisms synergistically amplify synaptic transmission and increase sensitivity, resulting in persistent pain. Moreover, the elevated intracellular calcium $(Ca^{2+})_i$ also stimulate many calcium-binding proteins that activate glial cells and trigger the production of pro-inflammatory cytokines and chemokines, which further heighten the sensitivity of pain pathways (Cho and Huh 2020, Jager, Goodwin et al. 2024). Therefore, it is essential to evaluate the temporal changes in $(Ca^{2+})_i$ in the animal model of NP which would provide in-depth knowledge about the role of calcium in the development of NP phenotypes.

Sciatica pain is a clinical medical ailment caused due to compression of the SN, resulting in pain that radiates down from the hip. It is characterized by paresthesia and numbness in the afflicted limb. This clinical illness is similar to the preclinical NP induced by chronic constriction injury (CCI) animal model where loose ligatures are

tied around the common SN that constricts the nerve without altering the epineural blood flow (Bennett and Xie 1988). Compelling clinical evidence has highlighted increased levels of calcium-binding proteins i.e., S100 in the cerebrospinal fluid of patients suffering from sciatica (Brisby, Olmarker et al. 1999, Skouen, Brisby et al. 1999). In parallel, a recent study also found that S100b was elevated in individuals suffering from trigeminal neuralgia, representing all of the symptoms observed in people suffering from NP (Ito, Seki et al. 2023). Similarly, preclinically, there are reports on the enhanced expression of S100b in the SC post-spinal nerve transection with the rodents displaying behavioral hypersensitivity (Tanga, Raghavendra et al. 2006, Chen, Huang et al. 2020). Based on the above clinical and preclinical consolidated evidence, S100b is recognized as a pathophysiological marker for persistent pain caused by nervous system damage. However, there is no information on the time-dependent changes in S100b in NP. Hence, the aim of the present study was to evaluate the temporal changes in $(Ca^{2+})_i$ level as well as calcium-binding protein (S100b) in rats with CCI-induced NP. This analysis will provide valuable insights into the dynamics of disease pathophysiological progression and also will assist in identifying the optimal timing for interventions.

To validate our hypothesis, in the present study, NP was induced by CCI of SN in rats and the establishment of the symptoms of pain was confirmed by various behavioral tests. The temporal changes in the intracellular calcium $(Ca^{2+})_i$ and S100b levels in the SN and SC post-peripheral nerve injury were elucidated. Following this, the validation of the involvement of S100b in the development and progression of NP was performed for the first time using a specific S100b inhibitor i.e., pentamidine in the CCI-induced NP model. To evaluate the sensory and motor abnormalities associated with NP, we

employed a range of behavioral tests to assess the effect of pentamidine. Then the effects of pentamidine on the $(Ca^{2+})_i$ and S100b level were evaluated post-CCI injury. In addition, we assessed the impact of pentamidine on the level of pro-inflammatory cytokines. We also quantified the expression levels of the markers of astrocytes and microglial activation i.e., GFAP and Iba-1 in SN and SC post-SN injury and the effects of pentamidine on them. To investigate the axonal damage, we performed analyses involving NF-L-positive staining of SN. Moreover, we explored the alterations in the neuronal morphology in the CCI model and evaluated the effects of specific S100b inhibitor on them using Golgi-Cox staining. Additionally, we quantified myatrophy using hematoxylin and eosin staining in this model and evaluated the effects of pentamidine on it. **Figure 5.1** presents a graphical representation depicting the schematic diagram outlining the proposed hypothesis concerning the molecular mechanism underlying the pathogenesis of NP in a rat model induced by CCI of SN.

Hypothesis

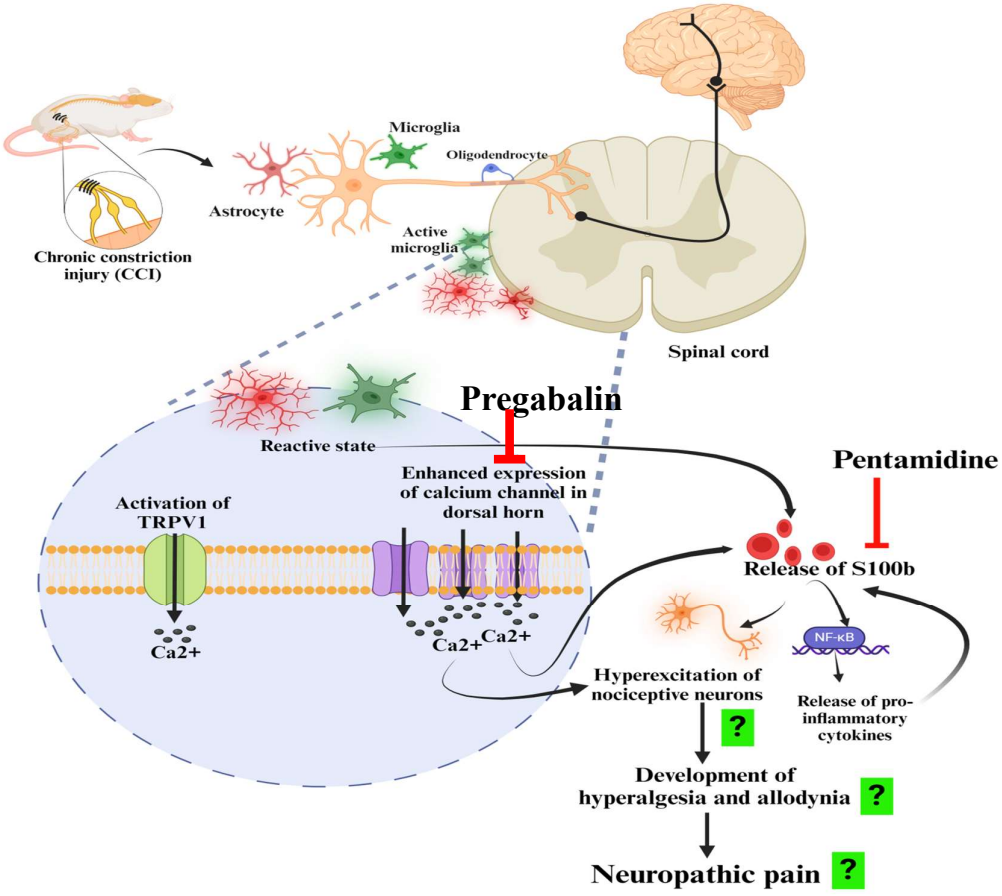

Figure 5.1. presents a graphical representation depicting the schematic diagram outlining the proposed hypothesis concerning the molecular mechanism underlying the pathogenesis of NP in a CCI-induced NP rat model. The injury to the sciatic nerve (SN) leads to the development of central sensitization due to upregulation in the expression of calcium channels ($Ca_V2.2$) in the dorsal horn of the spinal cord (SC). Besides, there are also enhanced expression of heat-sensing TRPV1 channels in the SC. Upregulation in the expression of these channels results in an increase in the influx of calcium ions leading to hyperexcitation of the nociceptive neurons and the development of NP phenotypes. In addition, the resident immune cells of CNS i.e., glial cells (astrocytes and microglia) get activated post-CCI leading to an increase in the release of calcium-binding proteins i.e., S100b. S100b gets activated in the presence of calcium ions causing the release of pro-inflammatory cytokines and progression of NP. Therefore, the temporal changes in the intracellular calcium and S100b protein level will help to identify the pharmacological window of oppourtunity. Besides, to validate the the role of S100b in the pathogenesis and progression of NP in this model, we have used a specific S100b inhibitor i.e., pentamidine to evaluate its effect on NP phenotypes.

5.1. Materials and methods

5.1.1. Materials

The molecular biology kits and reagents used in the qPCR experiment include TRI reagent & DEPC that was sourced from Sigma. The revert aid cDNA synthesis kit (Thermo Scientific), TURBO DNA-*free*^{TM} (Ambion), TURBO DNA-free™ Kit (Invitrogen), Maxima SYBR Green/ ROX qPCR master mix 2X and primers (Eurofins Genomics India), Prestained protein MW marker (Puregene) and 100bp DNA marker (MBI Fermentas), 6X DNA loading buffer (Thermo Scientific), and RNAase cocktail (Invitrogen) was used in this study. All the primer sequences used (**detailed in Table 5.1**) were sourced from Eurofins Scientific. Triton X-100, Dabco, 3-aminopropyltriethoxysilane, and formaldehyde were acquired from Sigma, USA. Tween-20 was purchased from Merck and DAPI was obtained from SRL. Fura2 AM was purchased from ChemCruz. For the study, the ELISA kits used were from Krishgen Biosystems. The primary antibodies used in the experiment are GFAP (No.: ab7260, Abcam), S100b (No. E-AB-60087; Elabscience Biotechnology Co., Ltd., USA), NF-L (No. CST-2837T; Cell Signaling Technology), and Iba1 (No. 019-19741; FUJIFILM Wako Chemicals U.S.A.). The secondary antibodies used are goat anti-rabbit IgG FITC (ab6717; Abcam) and goat anti-rabbit IgG TRITC (ab6718, Abcam).

5.1.2. Experimental animals and their ethical statement

Adult male Wistar albino rats of weight 200±20 g was used in the experiment that was obtained from the Central Animal House, IMS-BHU, Varanasi, India. Before starting the experiment, the rats were acclimatized for a week at an ambient and controlled temperature of 25±1°C with a 12-h light and dark cycle. The experimental animals had

ad libitum access to standard laboratory diet and water throughout the experiment. The rats were housed in cages (430 x 270 x 150 mm) with corn cob bedding. All the efforts were made to minimize the number of animals used during the experiment. The studies were performed in accordance with the guidelines of the Committee for the Control and Supervision of Experiments on Animals (CCSEA), Government of India and "Care and Use of Experimental Animals" (Vol.1, 2nd ed., 1993, and Vol.2, 1984) guidelines of National Institute of Health, U.S.A. The experimental protocol for the present study was approved by the Institutional Animal Ethical Committee (Ref No. IIT(BHU)/IAEC/2022/038 and IIT(BHU)/IAEC/2023/II/027).

5.1.3. Chronic constriction injury (CCI) model of Neuropathic pain

The NP was induced in the rats by CCI of the sciatic nerve (Bennett 1993). The experimental animals were anaesthetized intra-peritoneally using ketamine (80 mg/kg) and xylazine (10 mg/kg). Once the surgical level of anesthesia was attained, the rats were placed on the thermo-regulated heating mat maintained at 37°C. Then the skin of the right leg was shaved and sterilized and an incision parallel to the femur was made. The sciatic nerve was exposed by a gluteal muscle incision. Around 10 mm of the sciatic nerve proximal to the trifurcation was freed from the surrounding connective tissue and four loose ligatures (silk 4/0; Ethicon, USA) were tied with a gap of 1 mm around the nerve. The constriction of the sciatic nerve while tying the ligatures was done till a brief twitch was observed to prevent obstruction of the epineural blood flow. Then the muscle was sutured using 6/0 reabsorbable suture and the animals were kept under post-operative care. In order to limit the local infection, an iodine solution was applied prior to and after the suturing of the incision (**Figure 5.2)**.

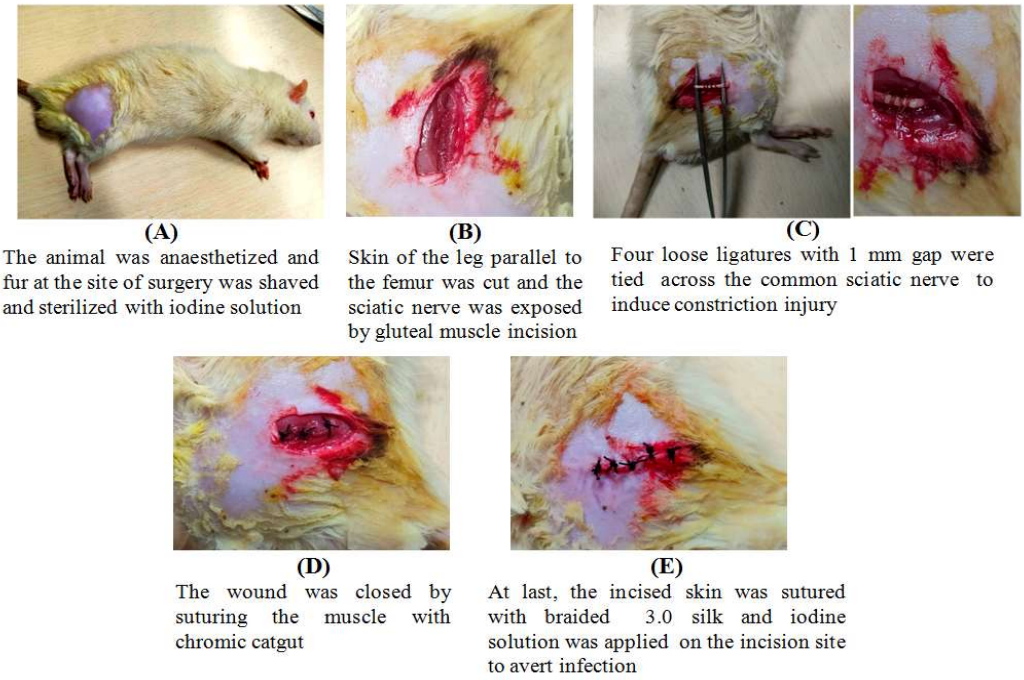

Figure 5.2: Schematic representation of the experimental protocol followed for the CCI-induced neuropathic pain model and the behavioral assessment of the symptoms developed post-surgery.

5.1.4.1. Animal experimental design for the temporal study to measure the changes in the intercellular calcium $(Ca^{2+})_i$ and S100b level

G*power analysis was conducted prior to designing the experimental protocol to determine the proper sample size, ensuring that the type I and II errors are kept under the acceptable threshold as suggested by Cohen (Cohen 1988). All the Wistar rats were weighed and were randomly divided into groups based on the time points when the rats were euthanized i.e., (i) D-0, (ii) 0.25, (iii) 0.5, (iv) 1, (v) 3, (vi) 7, (vii) 14, and (viii) 21 days post-CCI injury using the randomization technique. Each group had four animals (n= 4 rats/ group. NP was induced by CCI and behavioral assessments (hot-plate test, Randall Selitto test, acetone drop test, and BBB (Basso, Beattie, and Bresnahan) test) were performed before the surgery (D-0) and on days 3, 7, 14, and 21 post-surgery to access pain along with the motor and sensory deficits developed. On

the above-mentioned time intervals, the anaesthetized animals were sacrificed by decapitation (3% v/v isoflurane inhalation; R620 veterinary anesthesia machine, RWD life science, San Diego, USA). The SN of the ipsilateral side of the leg and SC were harvested. The dissected tissues were immediately stored at -80 °C until further research. The tissues collected were processed for biochemical analysis to measure the $(Ca^{2+})_i$ and S100b protein levels (**Figure 5.3)**.

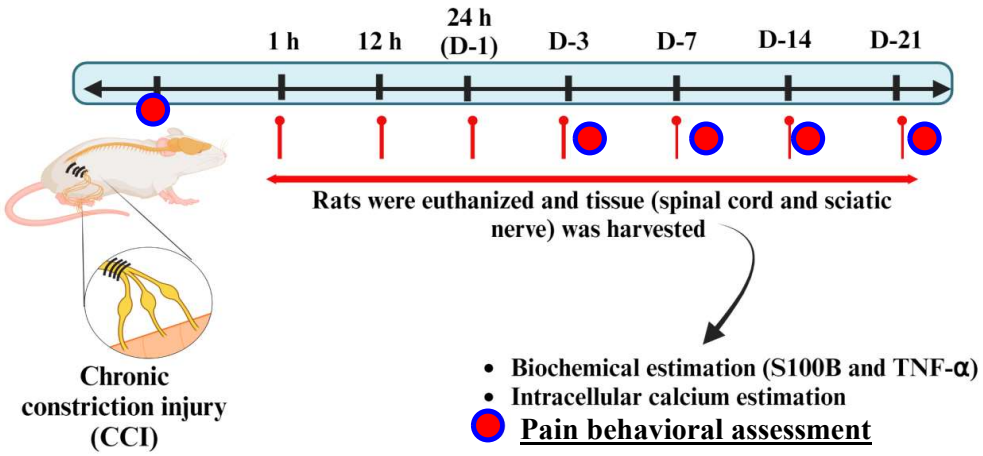

Figure 5.3: Schematic representation of the experimental protocol followed for the temporal study performed to measure the intracellular calcium and S100b level in the CCI-induced neuropathic pain model.

5.1.4.2. Animal experimental design for validation of the role of S100b in the pathogenesis/progression of NP

G*power analysis was conducted prior to designing the experimental protocol to determine the proper sample size, ensuring that the type I and II errors are kept under the acceptable threshold as suggested by Cohen (Cohen 1988). The current research consisted of 5 groups and by using A priori power analysis and ANOVA (repeated measures within-between interactions) statistical test, the minimum required sample size was determined to be 12. Consequently, we selected 12 male Wistar rats for each

group (n=12 rats/ group). All the Wistar rats were weighed and were randomly divided into five groups i.e., control, sham, CCI, CCI + pentamidine (10 mg/kg; i.p.), and CCI + pregabalin (30 mg/kg; p.o.) using the randomization technique. NP was induced by CCI and behavioral assessments like the hot-plate test, Randall Selitto test, acetone drop test, cotton swab test, Rota rod test, sciatic functional index (SFI), and BBB (Basso, Beattie, and Bresnahan) test) were performed before the surgery (D-0) and on days 7, 14, and 21 post-surgery to assess pain along with the motor and sensory deficits developed. On day 21, following the behavioral experiments, the animals were anaesthetized and sacrificed by decapitation. Then SN and SC were harvested and were immediately stored at -80 °C until further research (**Figure 5.4)**.

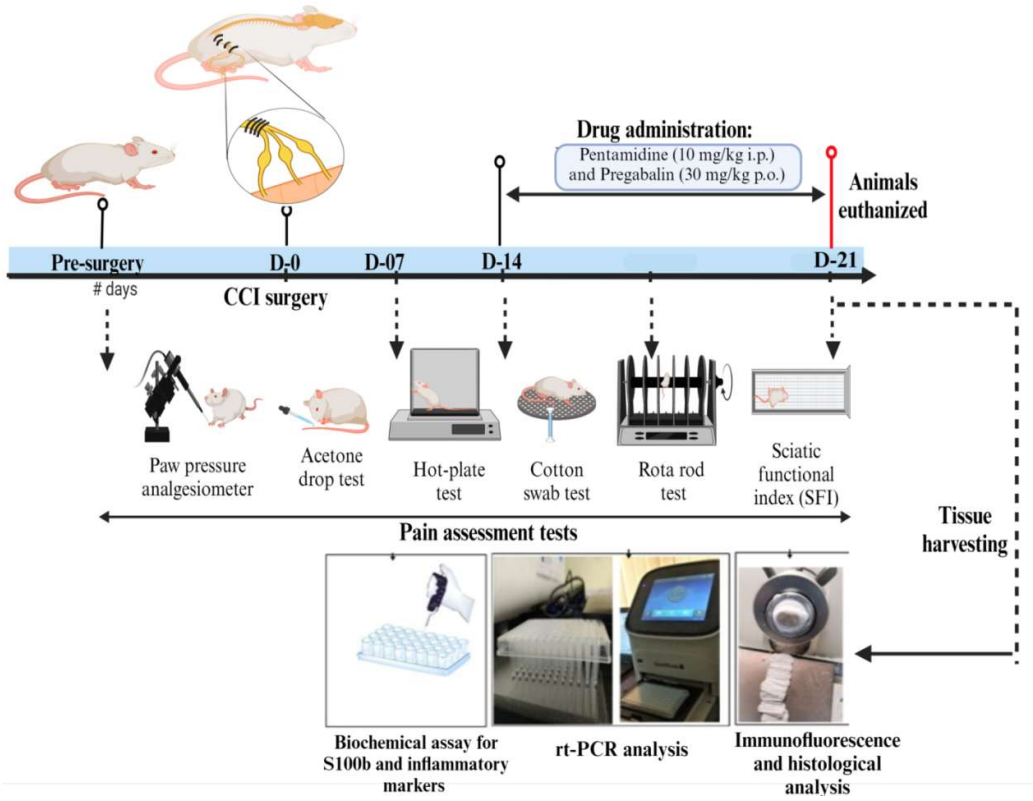

Figure 5.4: Schematic representation of the experimental protocol followed for validation of the role of S100b in the pathogenesis/progression of NP in the CCI-induced NP model in rats.

5.1.5. Behavioral analysis:

The experimental animals were acclimatized to the testing environment before the baseline behavioral testing. The development of NP phenotypes was assessed on days 7, 14, and 21 post-surgery.

5.1.5.1. Thermal hyperalgesia (hot-plate test)

The development of heat hyperalgesia in rats post-surgery was assessed using Eddy's hot plate (Orchid Scientific, India) (Khangura, Bali et al. 2017). The surface of the plate was preheated and the temperature was maintained at 52.5 ± 0.5 °C. Then animals were positioned on the heated plate and the nocifensive withdrawal reflex latency like uplifting and licking the rear paw of the injured side was recorded as the nociceptive threshold. The cut-off time of 20 sec was maintained to avoid burn injury to the animals.

5.1.5.2. Cold allodynia (acetone drop test)

The development of pain sensation due to non-noxious stimuli (cold) post-CCI surgery was evaluated by the acetone drop test. In this test, rats were first acclimatized in a chamber with a mesh floor for 20 min and then 100 μL of acetone was dropped on the dorsal surface of the hind paw of the injured leg. Cold allodynia produced in response to the evaporation of acetone is indicated by the repeated withdrawal, licking, biting, or flinching of the paw. The total duration of withdrawal of the paw in the air till it was placed back on the mess surface was recorded in seconds (Khangura, Bali et al. 2017).

5.1.5.3. Mechanical hyperalgesia (Randall Selitto test)

Hyperalgesia to the mechanical stimulation was measured in terms of the response of mechanical nociceptive threshold to the pressure applied on the paw of animals using

the digital paw pressure analgesiometer (Orchid Scientific, India) based on Randall Selitto test (Randall 1957, Ferrari, Rey et al. 2022). In this test, an increasing mechanical force is applied focally to the dorsal surface of the hind paw of the injured leg using the pressure applicator until a withdrawal nociceptive response is observed. The pressure at which the rats vocalized or displayed a painful response (flinching or withdrawal reaction of the paw or leg upon stimulation) was taken as the endpoint and recorded. The nociceptive threshold was defined as the mean of 3 subsequent readings, converted to force in grams.

5.1.5.4. Dynamic mechanical allodynia (Cotton swab test)

The dynamic mechanical allodynia developed after the CCI-induced NP were detected by the cotton swab test in rats (Field, Bramwell et al. 1999). The animals were first habituated in the plexiglass chamber with mesh flooring before the test session in order to minimize the normal movements during the test period. Then using a cotton swab, the planter part of the ipsilateral hind paw of rats was stroked gently and the latency of paw withdrawal was recorded with a cut-off time of 15 sec.

5.1.5.5. Rota rod

The rotarod test has been employed for assessing rats' motor coordination capability post-surgery (Prajapati, Garabadu et al. 2017). The animals being studied are trained for consecutive two days on the Rota rod (IKON instruments, India) at the lowest speed (i.e., 5 rpm) so that they attain stable baseline performances. Then, during the test session, the speed of the rotating rod was increased to 15 rpm. The total time spent by the animals on the rod was recorded with maximum a cut-off time of 300 sec.

5.1.5.6. Sciatic functional index (SFI):

SFI was calculated using the walking track analysis in which the animals were made to walk on a straight track (8.3 X 43 cm) that was darkened at one end (de Medinaceli, Freed et al. 1982, Komirishetty, Areti et al. 2017). The SFI value ranges from 0 to -100, with an SFI value 0 means normal while -100 denotes total impairment. After two or three trials on the track, the rats were conditioned so that they walked directly to the darkened end without exploring the track. Then a piece of white paper was placed on the walking track and the hind paws of the animals were dipped in different color solutions (the normal left paw with green and the injured right paw with red). The animal was then placed at the entrance of the track and was allowed to walk over the paper. The marks on the paper were dried and the following measurements were made:

Print length (PL): The length of one foot print of normal (NPL) and experimental side (EPL).

Total spreading (TS): The linear distance between the center of first toe print and the center of fifth toe print of normal (NTS) and experimental side (ETS).

Distance between intermediary toes (IT): The linear distance between the center of second toe print and the center of fourth toe print of normal (NIT) and experimental side (EIT).

The SFI was calculated using the following formula:

$$SFI = -38.8(EPL-NPL)/NPL + 109.5(ETS-NTS)/NTS + 13.3(EIT-NIT)/NIT – 8.8$$

5.1.5.7. BBB (Basso, Beattie, and Bresnahan) locomotor test:

BBB test is normally performed to assess the deterioration of the motor function post-CCI of the sciatic nerve in rats (Basso, Beattie et al. 1995). A score of 0 to 21 is given

according to the movement of the animal by a trained observer who was blinded to the experiment. A score of 0 was awarded when there was no spontaneous movement while a score of 21 when the rats showed normal limb movement. Normally score of 14 is given to an animal which showed complete limb coordination. In this experiment, the animals under study are placed in an open circular enclosure, observed for a period of 4 min and awarded scores accordingly.

5.1.6. Gastrocnemius muscle mass assessment:

The injury of the sciatic nerve leads to atrophy of the largest muscle supplied by it i.e., the gastrocnemius muscle which was assessed using the weight ratio of the gastrocnemius muscle 14 days after the surgery (Mohammadi, Amini et al. 2012). After the animals were euthanized, the gastrocnemius muscle was dissected from the contralateral and ipsilateral sides and weighed when still wet using an electronic balance.

5.1.7. Real Time quantitative PCR

Quantitative Real-Time PCR (qRT-PCR) was performed to assess the expression of the following genes at the mRNA level: NF-κB, $Ca_V2.2$, and TRPV1. For normalization, β-actin was used as a constitutive type control.

RNA isolation

To isolate total RNA from the SC and SN, we employed TRI reagent and followed a previously established protocol (Prajapati, Ahmed et al. 2024). Specifically, the tissues were homogenized in 1 mL of TRI reagent and centrifuged at 12,000 x g for 10 min at 4 °C. The resulting supernatant was collected, and 200 µL of chloroform was added. After vortexing for 15 s, the tubes were centrifuged again at 12,000 x g for 10 min at 4

°C, leading to the separation of three distinct phases: the phenol phase (containing nucleic acids), the protein phase (chloroform), and the colorless upper aqueous phase containing RNA. The colorless phase, containing RNA, was collected, and 0.5 mL of isopropanol was added to it. Following 5-min incubation, the tube was again centrifuged at 12,000 x g for 10 min at 4 °C. The RNA pellet formed at the bottom of the tube was then washed with 75 % ethanol, air-dried, and dissolved in 60 µL of DEPC-treated water.

DNase treatment

To eliminate any potential DNA contamination, the RNA was subjected to DNase treatment using the DNA-free Ambion. For each 20 µL of RNA extract, 2.5 µL of 10X DNase buffer, 0.5 µL of DNase enzyme, and 2 µL of DEPC-treated water were added. The mixture was then incubated for 30 min at 37 °C. Subsequently, 5 µL of DNase inhibitor was added to halt the reaction. The clear aqueous phase obtained by centrifugation at 10,000 x g at room temperature was used for RNA quantification.

cDNA synthesis

The cDNA synthesis was performed using Revert Aid's first-strand cDNA synthesis kit(Thermo Fisher Scientific, USA), utilizing RNA samples with an A260/A280 ratio ranging from 1.8 to 2.0. Initially, a reaction mixture was prepared by adding 4 µg of RNA, 1 µL of random hexamer primer, and DEPC-treated water, resulting in a total volume of 12 µL. After a brief centrifugation, the following components were added: 4 µL of 5X reaction buffer, 1 µL of RiboLock™ Ribonuclease Inhibitor (20U/µL), 2 µL of 10 mM dNTP mix, and 1 µL of reverse transcriptase, resulting in a final volume of 20 µL. The reaction mixture was incubated at 25 °C for 5 min, followed by cDNA strand

synthesis at 42 °C for 60 min. To terminate the reaction, the mixture was heated at 72 °C for 5 min. Finally, the synthesized cDNA was stored at -80 °C for future use.

Real time qPCR

The real-time qPCR was done with an ABI Prism 7500 Sequence Detection System (PE Applied Biosystems, CA, USA). The PCR reaction mixture, with a total volume of 20 µL, was comprised of 1 µL of sample cDNA (diluted 1:10), 1 µL of 10 pmol forward and reverse primers, and 10 µL of 2X SYBR Green/ROX qPCR Master Mix (Thermo Fisher Scientific, USA). The mixture was then brought to the final volume using RNase-free water. The PCR conditions involved an initial denaturation step at 95 °C for 30 s, followed by 40 cycles of amplification at 95 °C for 5 s, and 60 °C for 20 s. The amplification of each cDNA was confirmed through melting curve analysis. For data analysis, the ΔΔCT method was employed, wherein the Ct values of the target genes were normalized to the Ct values of the reference gene β-actin, relative to a control sample (Schmittgen and Livak 2008).

Table 5.1: Primer sequences used for qRTPCR

Name	Primer sequences
NF-κB	F- 5'- GCGTTTCCGTTACAAGTGCGAGG -3' R - 5'- CCCCAGGAATACTGCCTGCAGAG -3'
Cav2.2	F- 5'- AGGCCAGACATGAAGACACACA -3' R - 5'- TTGCCTTCCTTGCTTGAGTCCT -3'
TRPV1	F- 5'- GAATGACACCATCGCTCTGC -3' R - 5'- AAGAGGGTCACCAGCGTCAT -3'
β-actin	F- 5'-AGACTTCGAGCAAGAGATGGC -3' R-5'GATTCCATACCCAGGAAGGAAGG -3'

5.1.8. Assessment of S100b, TNF-α, and IL-6 protein level in sciatic nerve and spinal cord

S100b (No: KLR1360, Krishgen Biosystems), TNF-α (No: KB3145, Krishgen Biosystems), and IL-6 ELISA Kit (No: KB3068, Krishgen Biosystems) were used in this study to quantitatively assess the protein levels in SN and SC following the manufacturer's instructions. The protein concentrations were determined using the Bradford method (Bradford 1976).

5.1.9. Immunofluoresence

SN and SC were fixed in 4 % paraformaldehyde for 24 h followed by the antigen retrieval protocol was performed by boiling the tissue samples in citrate buffer (pH 5.9) for 5 min. Then tissues were transferred into 15 %, 20 %, and 20 % sucrose solutions respectively. When the SN and SC sink to the bottom of the solution, the sucrose solutions were changed. Tissues were then placed on the OCT compound in a cryomold. The OCT-embedded cryomold was gently placed into the liquid nitrogen to freeze the entire tissue in an OCT block. The blocks were stored at -80 °C. The SC sections were cut into 5µm thick coronal sections and SN longitudinally on the slides coated with 2 % APES (3-aminopropyl triethoxysilane) using cryostat microtome (Leica, USA). For immunostaining, the boundaries were made using a PAP pen on the slides which were then washed with PBS three times, 5 min each. Following this, the tissue sections were permeabilized in 0.2% Triton X-100. Then blocking was done in a solution containing 1% BSA and glycine in PBST (PBS with 0.1 % Tween 20) and incubated for 1 h. The sections were then incubated in the primary antibody at 4 °C in a humid chamber. After washing 3 times in PBS, secondary antibody (conjugated with Alexa fluorochrome) incubation was done and counterstained with 1µg/mL of 4’6-diamidino-2-phenylindole

(DAPI). The slides were mounted in DABCO, sealed and observed under a fluorescence microscope (Olympus BX53). Images captured were analyzed using the Image J program (NIH, USA) (Prajapati, Ahmed et al. 2024).

5.1.10. Golgi –Cox Staining

Golgi-Cox staining is a neurohistological technique employed to examine the cytoarchitecture of the nervous system. In this study, we have adopted the method described by (Zaqout and Kaindl 2016) with some modifications as described previously (Khanna, Chakraborty et al. 2020).

5.1.10.1 General Precautions

- Before use, all glass and plastic wares were thoroughly rinsed with fresh ddH_2O.
- Metal instruments were avoided during the impregnation step.
- All solutions were stored in a cool and dark place. Transparent glass reagent bottles were covered with aluminium foil, or small bottles were placed in a light-proof covered box.
- Careful handling of all solutions was exercised due to their toxicity. Direct skin contact or inhalation of vapours was avoided by wearing gloves and conducting experiments under a chemical hood.
- Slides coated with 3% gelatin were used in the study.

5.1.10.2. Preparation of Solutions

Sample Impregnation solution:

To prepare the 5 % w/v impregnation stock solution, potassium dichromate ($K_2Cr_2O_7$), mercuric chloride ($HgCl_2$), and potassium chromate (K_2CrO_4) were dissolved in double-distilled water (ddH_2O). The resulting solutions were stored in bottles at room

temperature in the dark without disturbance for at least 48 h. This allowed the formation of precipitates which was filtered.

Tissue protection solution:

At first, 0.1 M Phosphate buffer with a pH of 7.2 was prepared. To prepare the tissue protectant solution 300 g of Sucrose, 10 g of polyvinylpyrrolidone (PVP40; Rolex), and 300 mL of ethylene glycol ($C_2H_6O_2$) was added to 500 mL of the phosphate buffer. The volume of the cryoprotectant was then adjusted to 1000 mL using ddH_2O. The solution was then kept at 4 °C in the dark for long-term storage.

Developing solution:

The developing solution contains 50%, 70%, 95%, and 100% ethanol; Xylene (C8H10); a mixture of 3:1 parts of ammonia: double-distilled water (ddH_2O); and a solution of 5 % sodium thiosulphate ($Na_2S_2O_3.5H_2O$) in ddH_2O. All of these solutions were stored at room temperature.

5.1.10.3. Procedure for staining

Impregnation

Rats were anesthetized and transcardial perfusion was performed using 1 x PBS. SC was dissected out and kept in the impregnation solution at RT for 7-10 days. To prevent excessive impregnation of neurons, use of 4 % PFA for perfusion was avoided.

Tissue protection

Each tissue samples were carefully moved from the impregnation solution to a fresh bottle containing 10-15 mL of tissue-protectant solution. After a period of 24 h, the

tissue protectant solution was replaced with a fresh one. The SC tissues were then kept at a temperature of 4 °C in a dark environment for an additional 4-7 days.

Sectioning

Tissue sections were cut using a vibrotome (Leica) with a thickness of 150 µm onto gelatin-coated slides. To remove any excess tissue protectant solution, gentle palm pressure was applied while blotting the sections with Whatman paper. Subsequently, the slides containing the sections were air-dried for 2-3 days.

Developing step

The following process was used for development:

1. The slides were initially washed twice with distilled water for 5 min each and then transferred to a staining jar containing 50 % ethanol and left for 5 min.
2. Subsequently, the slides were placed in the ammonia solution.
3. After the ammonia treatment, the slides were washed twice with distilled water.
4. Next, the slides were immersed in sodium thiosulfate solution for 10 min, followed by washing.
5. The sections were dehydrated by immersing them in a series of ethanol gradients.
6. The slides were then cleared by placing them in xylene.
7. After clearing, the sections were mounted with DPX mounting medium.

5.1.10.4. Quantification of dendritic branching and spine density

The neurons were reconstructed at 400X magnification in a 3D manner using an Olympus BX53 microscope equipped with a motorized stage (MAC 5000 XYZ), camera, Ludl's joystick with focus control (Ludl Electronic Products, USA), and

Neurolucida software (MBF Bioscience) running on a Dell workstation. Following the completion of 3D tracing, Sholl's analysis was performed using Neuroexplorer software (MBF Bioscience) to measure the number of intersections, and dendrite lengths in each segment (Zaqout and Kaindl 2016).

5.1.11 Measurement of intracellular calcium level

SN and SC tissues were minced and digested with digestion buffer (40 unit/ml papain, 2.4 unit/ml dispase II, and 2% penicillin-streptomycin in PBS). Then the single-cell suspension of the digested tissue samples was prepared. 500µl volume of cell suspension was incubated with fura-2/acetoxymethyl ester (ChemCruz; SC-203052A) for 30 minutes at 37 °C. FURA 2/AM is rapidly metabolized in the cell by cytoplasmic esterases yielding the active dye FURA 2 which was estimated by measuring the fluorescence at 340 nm and 380 nm in the kinetic mode. For blank, a similar protocol was followed without the cell suspension (Malgaroli, Vallar et al. 1987).

5.1.12. Histological analysis of gastrocnemius muscle

The gastrocnemius muscle was fixed in a 10 % buffered formalin solution which was sliced (5 µm) using the cryostat. Then the finely sliced sections were stained with hematoxylin followed by counterstaining with eosin. Then the tissue sections were dehydrated with a graded series of alcohol and mounted with dibutyl phthalate xylene (DPX). The slides were then observed under the microscope (Olympus, Japan) for any structural abnormalities (Majumdar and Krishnamurthy 2022).

5.1.13. Statistical analysis

All data are represented as Mean ± SD and the statistical analysis was performed using the GraphPad Prism 8. The behavioral tests such as hot-plate test, acetone drop test,

Randall Selitto test, cotton swab test, Rota rod test, the BBB score, and SFI performed during the validation of S100b using pentamidine was analyzed statistically using the two-way ANOVA followed by Bonferroni post-hoc test. However, the behavioral study and changes in the intracellular calcium and S100b level performed during temporal study was analyzed by one-way ANOVA followed by Tukey multiple comparison post-hoc test. For the immunofluoresence expression of proteins and other datasets, one-way ANOVA followed by Tukey's multiple comparison post-hoc tests was followed. Differences were considered statistically significant when the P value is < 0.05 in the overall data analysis.

5.2. Results and Discussion

5.2.1. Temporal study to evaluate the development of NP phenotypes and changes in the intracellular calcium and S100b protein level

5.2.1.1. Effect of CCI on the development of NP phenotypes during the temporal study

The behavioral tests were conducted on days 3, 7, 14, and 21 after the CCI surgery to assess the development and progression of NP in rats. Previously, it has been demonstrated that CCI animal models lead to increased sensitivity to pain (hyperalgesia) and also cause the development of allodynia (Bennett, Chung et al. 2003). Similarly, in our study, statistical analysis by one-way ANOVA followed by post-hoc test revealed the development of thermal hyperalgesia, cold allodynia, and mechanical hyperalgesia ($p < 0.05$) compared to the rats on D-7 after the surgery (as shown in **Figure 5.5**). The peripheral nerve injury caused a significant reduction in the withdrawal latency when placed on the hot plate (**Figure 5.5A)** along with the elevation

in paw withdrawal duration on dropping acetone on the injured paw (**Figure 5.5B)** among the groups ([$F(4,19) = 14.45$; $p < 0.05$] and [$F(4,19) = 20.52$; $p < 0.05$] respectively). Further, on D-14, there was a substantial increase in thermal hyperalgesia and cold allodynia compared to the rats before surgery (i.e., D-0), as well as on days 3 and 7 (D-3 and D-7) and a similar trend was observed until D-21. Post-injury to the SN often leads to an increase in the sensitivity of sensory nerve fibers that detects cold sensory inputs (Xing, Chen et al. 2007). Consequently, abnormal signaling may occur in response to temperatures, accurately reflecting clinical symptoms like cold allodynia in persons with peripheral neuropathy.

Further, it was also observed that the threshold to withstand the pressure applied on the dorsal part of the paw decreased significantly during the Randall Selitto test (**Figure 5.5C)** among the groups ([$F(4,19) = 15.54$; $p < 0.05$]). Over time, mechanical hyperalgesia gradually increased, reaching maxima on D-14 following which, a plateau was observed. The development of mechanical hyperalgesia in the CCI model can be explained due to the complex and overlaying interplay between the peripheral and central nervous systems mostly due to neuroplastic alterations in the SN and SC (Calvo, Dawes et al. 2012) that increases the ectopic discharges and excitability of nociceptive nerve fibres; hence, exacerbating the non-noxious sensory input (Chen, Tan et al. 2019). In extension, we also observed that post-CCI, there was development of motor in-coordination as evident from the statistically lower BBB score (**Figure 5.5D**) among the groups ([$F(4,19) = 107.5$; $p < 0.05$]). Similar to our observation, Bagriyanik et al. (Bagriyanik, Ersoy et al. 2014) reported that injury to the SN after CCI surgery produced significant changes in the neuromuscular coordination in rodents which is similar to the motor disability observed clinically (Goswami, Aleem et al. 2021).

Therefore, it can be affirmed that CCI of SN caused sensory and motor deficits in rats which started from D-7 and was maximum on D-14 following which the symptoms stabilized in this NP model.

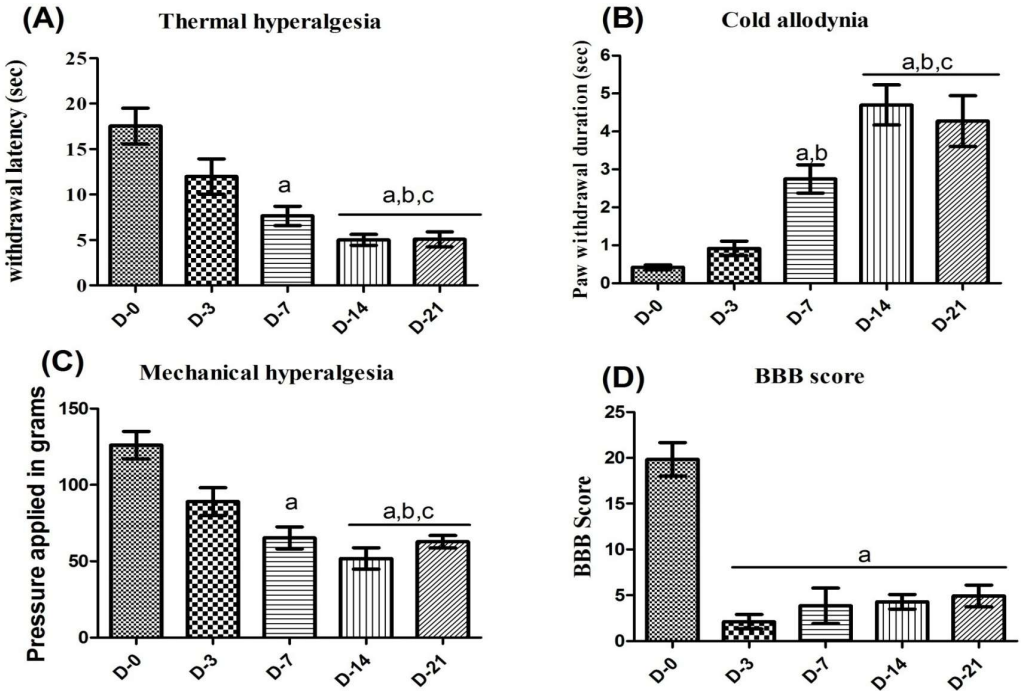

Figure 5.5: Sensory and motor deficit due to chronic constriction injury in rats. The effect of CCI on the development of (A) thermal hyperalgesia, (B) cold allodynia, (C) mechanical hyperalgesia, and (D) changes in the BBB score. All values are in mean ± SD (n=4 rats/ group). $^{a}p<0.05$, $^{b}p<0.05$, and $^{c}p<0.05$ compared to D-0, D-3, and D-7 respectively. (One-way ANOVA followed by Tukey multiple comparison post-hoc test)

5.2.1.2. Temporal changes in the intracellular calcium, S100b, and pro-inflammatory cytokine (TNF-α) level post-CCI of sciatic nerve

The development and maintenance of NP are significantly influenced by an increase in the intracellular calcium $(Ca^{2+})_i$ level as an increase in the influx of calcium causes neuronal hyperexcitability of the primary afferent neurons in the SN and SC (Hogan, McCallum et al. 2000) that perpetuates NP phenotypes. Thus, our investigation aimed to determine the changes in the $(Ca^{2+})_i$ level in order to identify the pharmacological

window of opportunity so that we can know the probable time window to start the treatment (**Figure 5.6**). In the CCI paradigm of NP, statistical analysis by one-way ANOVA followed by post hoc test revealed that there was a significant increase in the $(Ca^{2+})_i$ level in SN acutely 1 h after the surgery compared to the rats before surgery ((D-0); ([F(7,31) = 81.76; p <0.05])) (as represented in **Figure 5.6A)**. The $(Ca^{2+})_i$ level increased gradually and the maximum concentration was observed on D-14 following which it stabilized. However, in the SC, a significant increase in the $(Ca^{2+})_i$ level was observed on D-1 among the groups (([F(7,31) = 35.23; p <0.05]) as shown in **Figure 5.6D**. The $(Ca^{2+})_i$ level had further increased as observed in the SN with the maximum concentration on D-14. This corroborates with the pain behavioral assessment test performed where the sensory and motor deficits reached their peak on D-14, after which the symptoms in this NP model stabilized (**Figure 5.5**). The increase in the $(Ca_2^{+})_i$ has been reported to facilitate further increase in the influx of calcium through various ion channels leading to neuroplastic changes in the primary afferent fibres and glial cell-induced neuroinflammation that exacerbates pain (Kawamata and Omote 1996).

Similarly, injury to the PNS often leads to glial cell activation that is linked with the increase in calcium-binding protein i.e., S100b which plays a significant role in neuroinflammation and sensitization of the pain pathways. Therefore, the temporal changes in the S100b and pro-inflammatory cytokine (TNF-α) were evaluated in SN and SC. Statistical analysis by one-way ANOVA revealed significant changes in the S100b and TNF-α among the groups (([F(7,31) = 63.90; p <0.05] and ([F(7,31) = 109.4; p <0.05]) respectively) in SN. Post-hoc analysis indicates that the CCI rats demonstrated a significant increase in S100b and TNF-α from 12 h compared to the naïve rats (i.e., D-0) and the maximum concentration was observed on D-14 (**Figure**

5.6B and C). Likewise, in the SC, one-way ANOVA followed by post-hoc analysis data showed significant differences in S100b and TNF-α levels among the groups (([F(7,31) = 112.1; $p < 0.05$] and ([F(7,31) = 90.55; $p < 0.05$]) respectively) compared to the rats without SN injury (**Figure 5.6 E and F**). The observed elevated S100b level in SN may be associated with altered Schwann cell proliferation and Wallerian degeneration post-injury, thereby impacting the nerve regeneration process. While in SC, the excessive increase in S100b level compared to the control group can be linked with activated glial cells that lead to a heightened state of neuroinflammation and neuronal damage, contributing to persistent painful phenotypes. In the present study, we, for the first time report that there are time-dependent changes in the $(Ca^{2+})_i$ and S100b in the CCI model of NP in rats.

Additionally, the correlation between $(Ca^{2+})_i$, S100b and TNF-α level on D-21 post-CCI was performed and is illustrated in **Figure 5.7a**. S100b was significantly and positively correlated with $(Ca^{2+})_i$, and TNF-α ($p<0.05$). This implicates the involvement of $(Ca^{2+})_i$ and S100b in the regulation of inflammation in the CCI model in a time-dependent manner. Further, a significant positive correlation of S100b with NP phenotypes was observed (**Figure 5.7b**). Therefore, it is probable that S100b is involved in the progression of NP. Besides, S100b also regulates the neuroinflammation as TNF-α increases in a time-dependent manner.

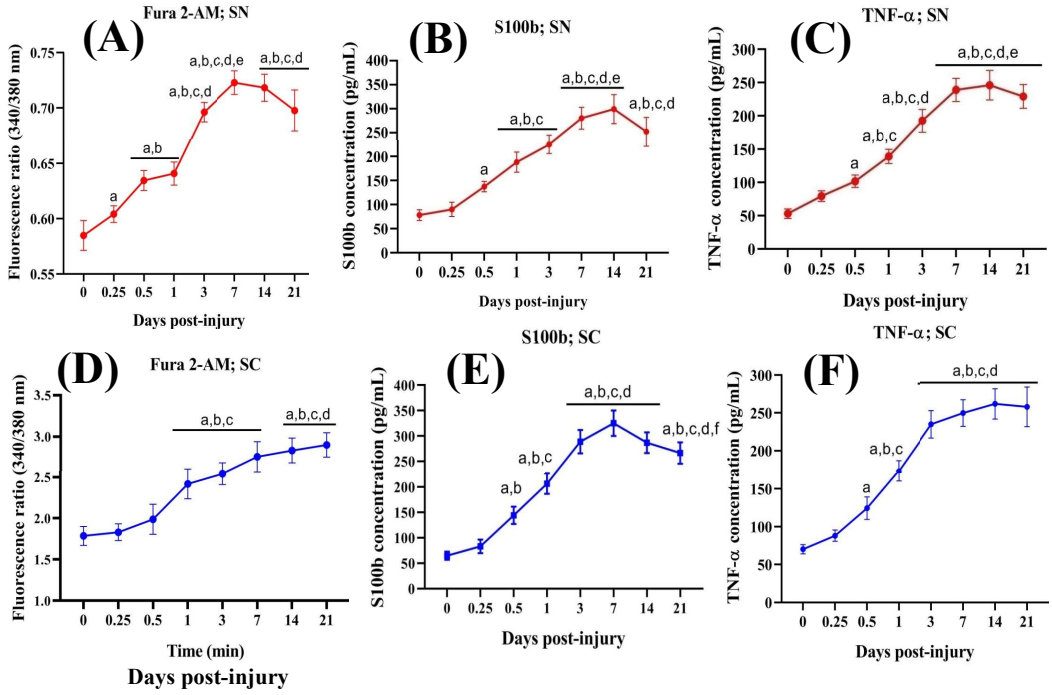

Figure 5.6: Temporal changes in the intracellular calcium, S100b and TNF-α level in SN and SC post-CCI injury. All values are in mean ± SD (n=4 rats/ group). [a]p<0.05, [b]p<0.05, [c]p<0.05, [d]p<0.05, [e]p<0.05, and [f]p<0.05 compared to 0, 0.25, 0.5, 1, 3, and 7 days post-injury. (One-way ANOVA followed by Tukey's multiple comparison post-hoc test)

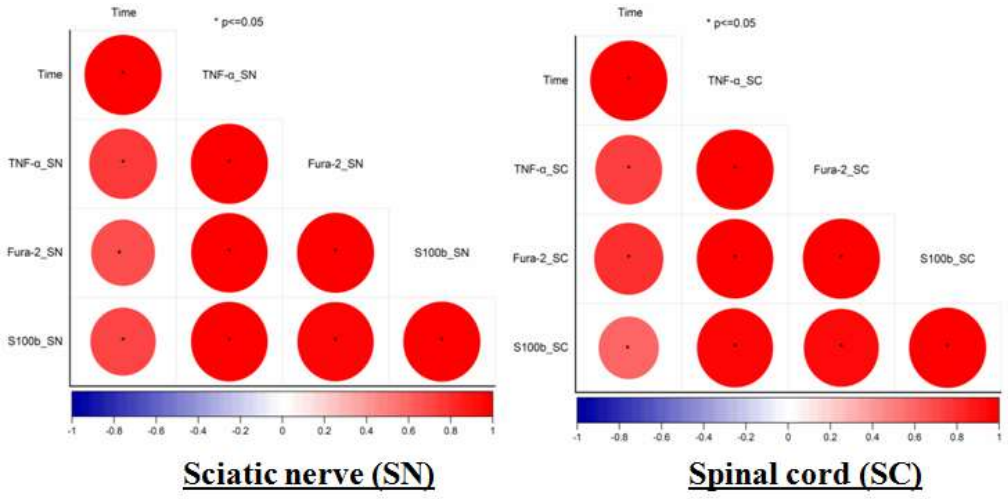

Figure 5.7a: A correlation between intracellular calcium level, S100b, and TNF-α level on D-21 post-CCI of peripheral nerve.

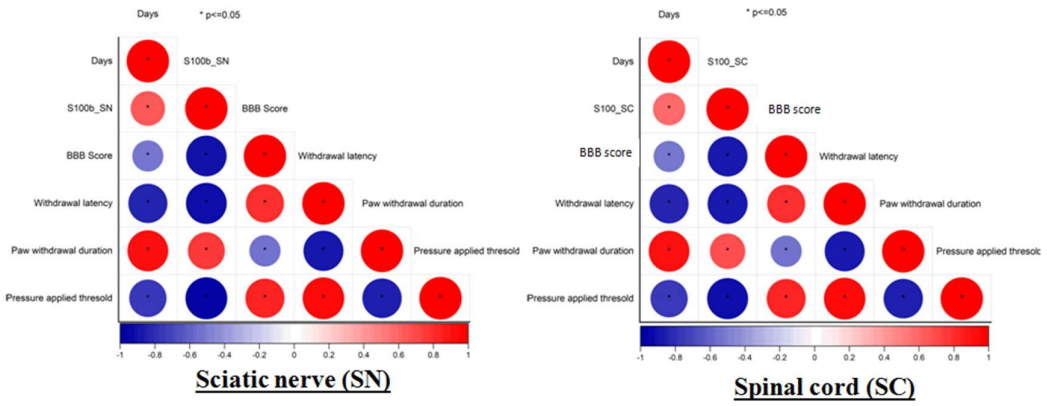

Figure 5.7b: A correlation between S100b level and NP phenotypes on D-21 post-CCI of peripheral nerve.

5.2.2. Validation of the role of S100b in the pathogenesis/progression of NP in rat CCI model

5.2.2.1. Effect of pentamidine on the CCI-induced sensory and motor deficits

CCI animal model induces the development of hyperalgesia and allodynia in response to various non-noxious stimuli. In the present study, statistical analysis by two-way ANOVA revealed the development of thermal hyperalgesia and cold allodynia among the groups ([F (4, 220) = 298.0; $p < 0.05$] and [F (4, 220) = 456.9; $p < 0.05$] respectively), time periods ([F (3, 220) = 205.4; $p < 0.05$] and [F (3, 220) = 363.4; $p < 0.05$] respectively), and the interaction between group and time ([F (12, 220) = 40.05; $p < 0.05$] and [F (12, 220) = 68.17; $p < 0.05$] respectively). Post-hoc test represented that there was a significant decrease in paw withdrawal latency when placed on the hot-plate with a simultaneous increase in paw withdrawal duration when acetone was sprayed on the paw of the injured leg following CCI compared to control from D-7 onwards till D-21 (**Figure 5.8A and B**). This finding is supported by a previous study, where CCI caused thermal and cold hypersensitivity in rodents similar to the clinically observed symptoms (Hamidi, Ramezani et al. 2012). Further, for the first time we

observed that the treatment with a specific S100b inhibitor i.e., pentamidine attenuated thermal hyperalgesia and cold allodynia similarly to pregabalin as observed on D-21. However, there were significant differences between the effects of pregabalin and pentamidine observed on these NP phenotypes. Notably, no significant differences in thermal hyperalgesia and cold allodynia were observed between the control and sham. Hence, the above results suggest that S100b is involved in the development and progression of NP symptoms in this model as a specific S100b inhibitor reversed these NP phenotypes.

Furthermore, chronic pain is clinically characterized by hypersensitivity induced by mechanical stimuli (Bannister, Sachau et al. 2020). Thus, in the present study, we have evaluated whether pentamidine can mitigate mechanical hyperalgesia and dynamic mechanical allodynia in the CCI model using Randall Selitto and cotton swab test (**Figure 5.8 C and D**). In the Randall Selitto and cotton swab paradigm, the pressure applied on the ipsilateral side and paw withdrawal latency was decreased after CCI ([$F(4, 220) = 256.8$; $p < 0.05$] and [$F(4, 220) = 366.4$; $p < 0.05$] respectively), with time ([$F(3, 220) = 240.6$; $p < 0.05$] and [$F(3, 220) = 251.9$; $p < 0.05$] respectively). Further, there was a significant interaction between groups and time ([$F(12, 220) = 34.55$; $p < 0.05$] and [$F(12, 220) = 45.26$; $p < 0.05$] respectively) in this paradigm. Post-hoc analysis revealed that there was a significant decrease in mechanical hyperalgesia and dynamic mechanical allodynia following CCI compared to the naïve rats from D-7 onwards till D-21. However, pentamidine reversed these CCI-induced NP phenotypes as observed on D-21 evident from a significant increase in the threshold to withstand the pressure applied compared to the untreated group. Similarly, Aδ fibre-mediated dynamic allodynia was also attenuated by pentamidine compared to the CCI rats. This

confirms that S100b plays a vital role progression of heterogeneous NP symptoms in this paradigm. Notably, there were no observed changes in the NP phenotypes in between the contralateral paws of rats after nerve injury and before CCI of SN and also following the drug treatment.

Moreover, we found motor deficits following the CCI and statistical analysis using repeated measures of two-way ANOVA revealed a significant differences in the rotarod retention time among the different groups [$F(4, 220) = 166.6$, $p < 0.05$] as well as over time [$F(3, 220) = 129.7$, $p < 0.05$]. Additionally, an interaction between group and time was also observed [$F(12, 220) = 24.75$, $p < 0.05$] as shown in **Figure 5.8E.** Similar to our observation, Bagriyaniket al. (Bagriyanik, Ersoy et al. 2014) reported that injury to the SN after CCI surgery produced significant changes in the neuromuscular coordination in rodents which is similar to the motor disability observed clinically (Goswami, Aleem et al. 2021). Post-hoc analysis showed CCI rats exhibited significant decrease in the retention time on the rotating rod compared to control animals from D-7 and was maintained till D-21 which was reserved by pentamidine treatment. In this context, a recent study reported that pentamidine improved motor impairment in a chronic experimental autoimmune encephalomyelitis model (Barros, Barateiro et al. 2022).

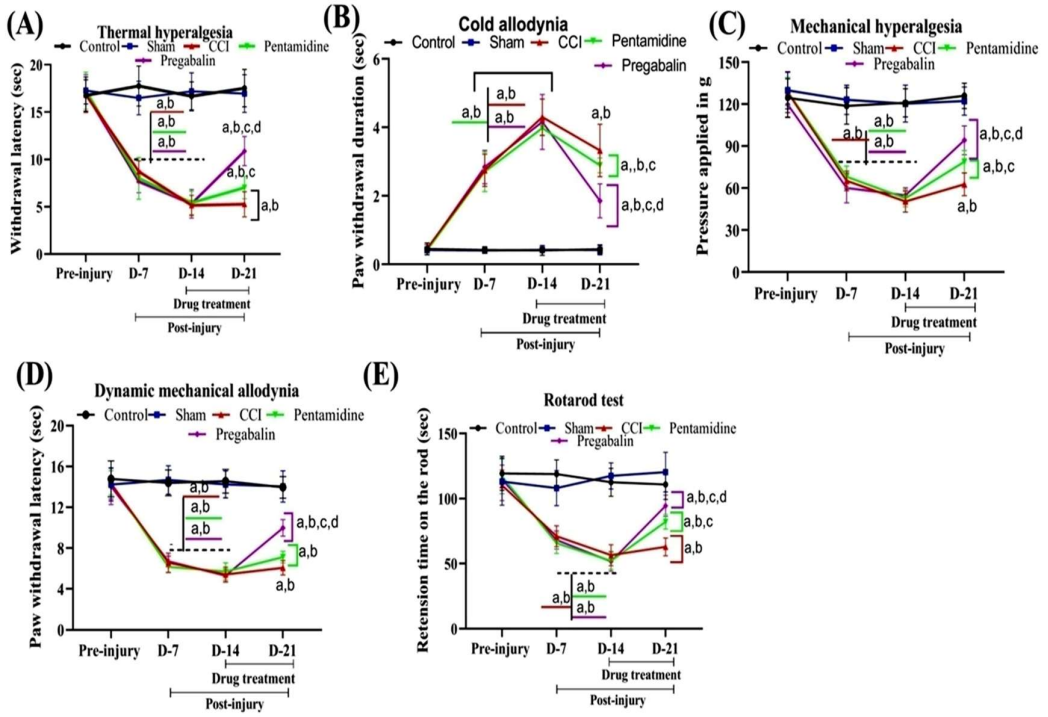

Figure 5.8: Sensory and motor deficit due to chronic constriction injury in rats. Effect of pentamidine on (A) thermal hyperalgesia, (B) cold allodynia, (C) mechanical hyperalgesia, (D) dynamic mechanical allodynia, and (E) retention time on the rota-rod. All values are in mean ± SD (n=12 rats/ group). $^{a}p<0.05$, $^{b}p<0.05$, $^{c}p<0.05$, and $^{d}p<0.05$ compared to control, sham, CCI, and pentamidine respectively. (Two-way ANOVA followed by Bonferroni post-hoc test)

5.2.2.2. Effect of pentamidine on the CCI-induced motor coordination

The impairment in motor coordination post-injury to the peripheral nerve along with the evaluation of the functional condition of the injured SN was performed using the BBB score and SFI (**Figure 5.9**). Post-CCI, we observed that the injured hind paw was awkwardly positioned when walking, and the toes were somewhat ventroflexed and the rodents walked with an obvious limp as shown in **Figure 5.9i**. The hind paw was everted and the animal stood and walked with the full medial border of its hind paw contacting the ground. However, post-treatment, there was an improvement in the gait with less limping observed. **Figure 5.9iiB** below illustrates the effect of pentamidine on BBB Score and SFI in CCI rats. Statistical analysis by repeated measure two-way

ANOVA revealed significant differences in BBB Score and SFI among the group ([F (4,220)= 2413; P<0.05] and [F (4,220)= 1478; P<0.05] respectively), time [F (3, 220)=1840; P<0.05] and [F (3,220)= 997.4; P<0.05], respectively) and a significant interaction between groups and time ([F (12,220)=334.0]; P<0.05] and [F (12,220)= 181.6; P<0.05] respectively). The control and sham groups did not exhibit significant differences according to the post hoc analysis. The SFI of the CCI rats on day 14 was found to be -77.67 ± 10.01 compared to 5.98 ± 1.03 before surgery. Previously, studies have also reported that ligation of the SN produced a reduction in the total spreading of the paw with an increase in print length and hence decreased SFI, denoting functional deficits of the nerve and development of walking impairment due to pain (Wang, Chen et al. 2021). Therefore, it can be affirmed that CCI caused sensory and motor deficits in rats along with the development of NP phenotypes. However, treatment with pentamidine restored the motor function as the SFI improved to -61.85 ± 8.11 after seven days of treatment. Hence, together with the improvement in the BBB score, these findings confirm that the specific inhibitor of S100b not only mitigated the core symptoms of NP but also improved motor performances in the CCI model.

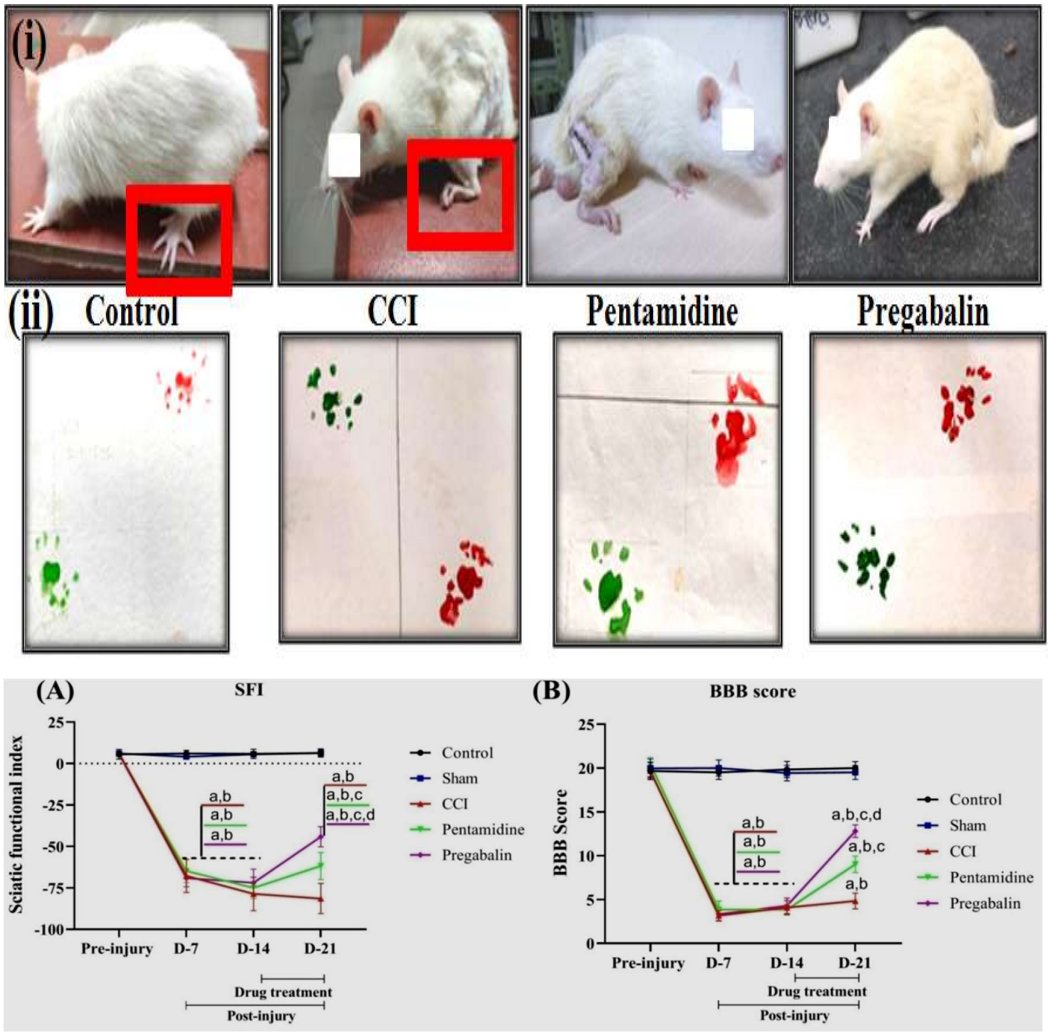

Figure 5.9: Representative images of the (i) paw of the ipsilateral side and (ii) footprints of control, CCI, pentamidine and pregabalin treated rats. (ii) Effect of pentamidine on SFI and BBB score. All values are in mean ± SD (n=12 rats/ group). $^{a}p<0.05$, $^{b}p<0.05$, $^{c}p<0.05$, and $^{d}p<0.05$ compared to control, sham, CCI, and pentamidine respectively. (Two-way ANOVA followed by Bonferroni post-hoc test)

5.2.2.3. Effect of pentamidine on the intracellular calcium $(Ca^{2+})_i$ and S100b level in SN and SC

Increased $(Ca^{2+})_i$ levels play a crucial role in the development of NP as it increases neuronal excitability, stimulates the release of neurotransmitters, triggers pro-nociceptive pathways along with the activation of downstream cascades that facilitate further release of calcium and exacerbates painful phenotypes (Cui, Wu et al. 2021).

Further, a series of studies reported that post-tissue injury, the calcium-binding protein (S100b) is actively released from the activated glial cells creating a pro-inflammatory environment that contributes to the pathophysiology of any disease (Michetti, Di Sante et al. 2021, Michetti, Clementi et al. 2023). Similarly, in our study, we have observed that there was a time-dependent increase in the $(Ca^{2+})_i$ and S100b levels in both SN and SC post-injury to the SN (as shown in **Figure 5.6**). As a result, our study sought to determine if the administration of a specific S100b inhibitor will result in the reduction of $(Ca^{2+})_i$ level post-CCI of SN. To analyze the effects of pentamidine on $(Ca^{2+})_i$ level and to identify the significant differences among the groups, statistical analysis by one-way ANOVA was employed ([$F(4,19) = 20.97$; $p<0.05$] and ([$F(4,19) = 24.41$; $p<0.05$] respectively). Post-hoc analysis revealed a significant increase in $(Ca^{2+})_i$ level in both SN and SC following CCI compared to control and sham rats. Pregabalin, a CCB and the first-line treatment for NP significantly mitigated the increased $(Ca^{2+})_i$ level as observed on D-21. Interestingly, unlike pregabalin, treatment with pentamidine did not significantly alter the elevated $(Ca^{2+})_i$ level post-injury (**Figure 5.10iA and B**).

Furthermore, in our study, one-way ANOVA revealed a difference in S100b level post-treatment with pentamidine in SN [$F(4,19)= 156.7$; $p<0.05$] and SC [$F(4,19)= 280.2$; $p<0.05$] among the groups. Tukey's post-hoc test showed a significant increase in S100b level in both SN and SC following CCI compared to the control group. Notably, there were no significant differences in the S100b level between the control and sham rats. Nevertheless, following 7 days of treatment with pentamidine, we observed a significantly decreased S100b level in both SN and SC by 2.2-fold. However, the group that received pregabalin exhibited no significant differences compared to the disease group (**Figure 5.10iiA and B**). Additionally, the correlation between S100b and NP

phenotypes after the pentamidine treatment (10 mg/kg b.w.) revealed that they are positively correlated ($p<0.05$) (**Figure 5.11**). Therefore, our investigation suggests that pentamidine attenuated the core symptoms of NP phenotypes in the CCI model by regulating the S100b.

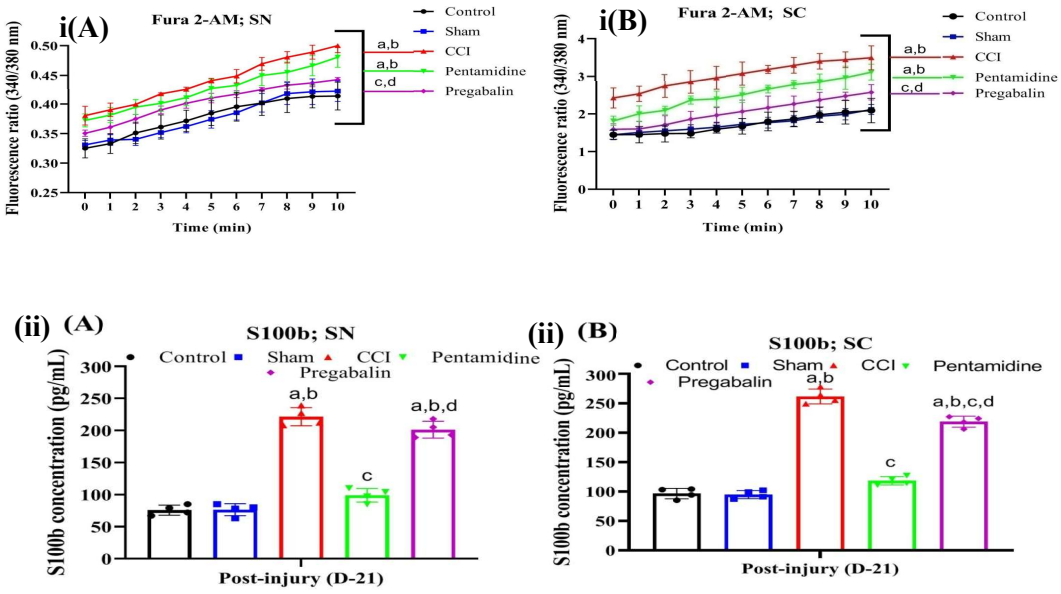

Figure 5.10: Effect of pentamidine on (i) intracellular calcium and (ii) S100b level in SN and SC. All values are in mean ± SD (n=4 rats/ group). [a]$p<0.05$, [b]$p<0.05$, [c]$p<0.05$, and [d]$p<0.05$ compared to control, sham, CCI, and pentamidine respectively. (Two-way ANOVA followed by Bonferroni post-hoc test for Fura 2-AM assay) (One-way ANOVA followed by Tukey's multiple comparison post-hoc tests for S100b level)

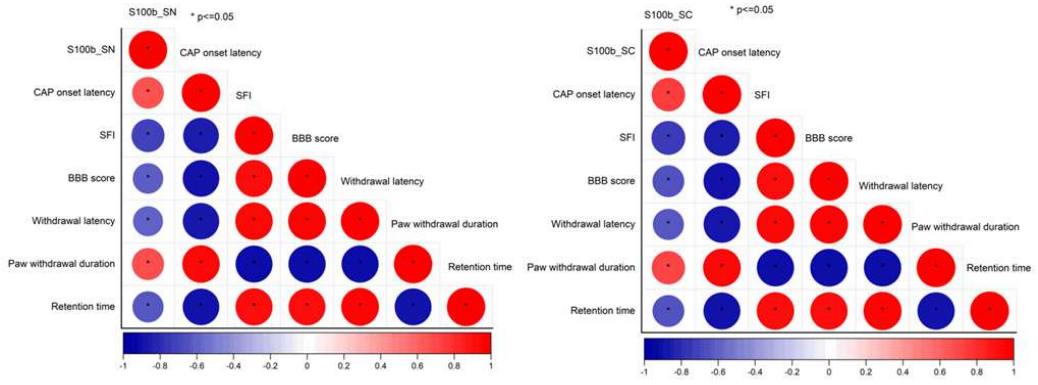

Figure 5.11: A correlation between S100b and NP phenotypes after the pentamidine treatment (10 mg/kg b.w.)

5.2.2.4. Effect of pentamidine on the $Ca_V2.2$ and TRPV1 mRNA expression in SN and SC

In the present study, we have analyzed the $Ca_V2.2$ and TRPV1 mRNA expression in the SN and SC as there were enhanced levels of $(Ca^{2+})_i$ observed post-CCI (illustrated in **Figure 5.10**). Statistical analysis revealed that there was a significant increase in the fold change mRNA expression of $Ca_V2.2$ among the groups in both SN and SC ([$F(4,19) = 57.57$, $p<0.05$] and $F(4,19) = 187.3$, $p<0.05$] respectively). The post-hoc test showed an increase in $Ca_V2.2$ expression following injury to the peripheral nerve compared to the control and sham groups. The over-expression of $Ca_V2.2$ has also been observed previously in rats with CCI-induced NP (Luo, Calcutt et al. 2002, Bucci, Mochida et al. 2011, Cai, Quan et al. 2022) leading to a persistent influx of calcium in the primary afferent terminals (Alles, Garcia et al. 2018). This reportedly activates downstream cascade pathways of synaptic vesicle fusion with the antidromic release of neurotransmitters, contributing to the positive feedback mechanism of peripheral sensitization (Cai, Quan et al. 2022). Besides, elevated intracellular calcium level also results in long-term potentiation of nociceptive transmission to spinal and supraspinal regions causing central amplification of pain (Sun, Tong et al. 2022). Elevated $(Ca^{2+})_i$ level is also involved in glial cell activation especially astrocytes that contributes to the release of gliotransmitters that modulate neuronal activity and pain perception (Cho and Huh 2020). Treatment with a CCB i.e., pregabalin caused a significant decrease in the $Ca_V2.2$ expression compared to untreated NP rats (**Figure 5.12 (A and B)**) along with the reversal of abnormal rise in $(Ca^{2+})_i$ post-injury to the peripheral nerve. However, a specific S100b inhibitor (pentamidine) reduced the CCI-induced increase in the $Ca_V2.2$ mRNA expression in the SN and SC but was not as effective as pregabalin. Therefore,

the analgesic effects of pentamidine observed in the CCI-induced NP model are more associated with S100b regulation as corroborated by the reversal of the NP phenotypes observed after pentamidine treatment (**Figure 5.8**).

Furthermore, in our study, one-way ANOVA revealed a difference in the mRNA expression of TRPV1 (Transient receptor potential vanilloid 1) post-treatment with pentamidine among the groups in the SN ($F(4,19) = 231.3$, $p<0.05$]) and SC ($F(4,19) = 105.6$, $p<0.05$]). Tukey's post-hoc test showed a significant increase in TRPV1 expression in both SN and SC following CCI compared to the control group. TRPV1 is a calcium-permeable ion channel that is predominantly expressed in the sensory neurons and is primarily involved in sensing temperature > 43 °C (Malek, Pajak et al. 2015). During NP conditions, TPRV1 are reportedly upregulated in the C and A-fibers after peripheral nerve injury leading to the development of thermal hyperalgesia (Huang, Lu et al. 2020). This is coherent with our study where CCI of SN led to the development of thermal hyperalgesia in rats (**Figure 5.8**). Besides, there are previous studies providing links between TRPV1 upregulation, glial cell activation and development of hypersensitivity to thermal stimuli in various NP animal models (Chen, Willcockson et al. 2009). TRP channels have also been identified in regulating the calcium ion homeostasis (Lee, Jo et al. 2021) and aberrant changes in the expression of TRPV1 following the peripheral nerve injury may lead to excessive release of calcium-mediated neurotransmitters causing sensitization of path pathways and exaggerate the pain sensation. However, treatment with pregabalin and pentamidine produced a significant decrease in the TRPV1 mRNA expression in SN and SC compared to the CCI group (**Figure 5.12(C and D**)). Therefore, inhibiting S100b using pentamidine mitigated thermal hypersensitivity by alleviating the TRPV1 expression in SN and SC.

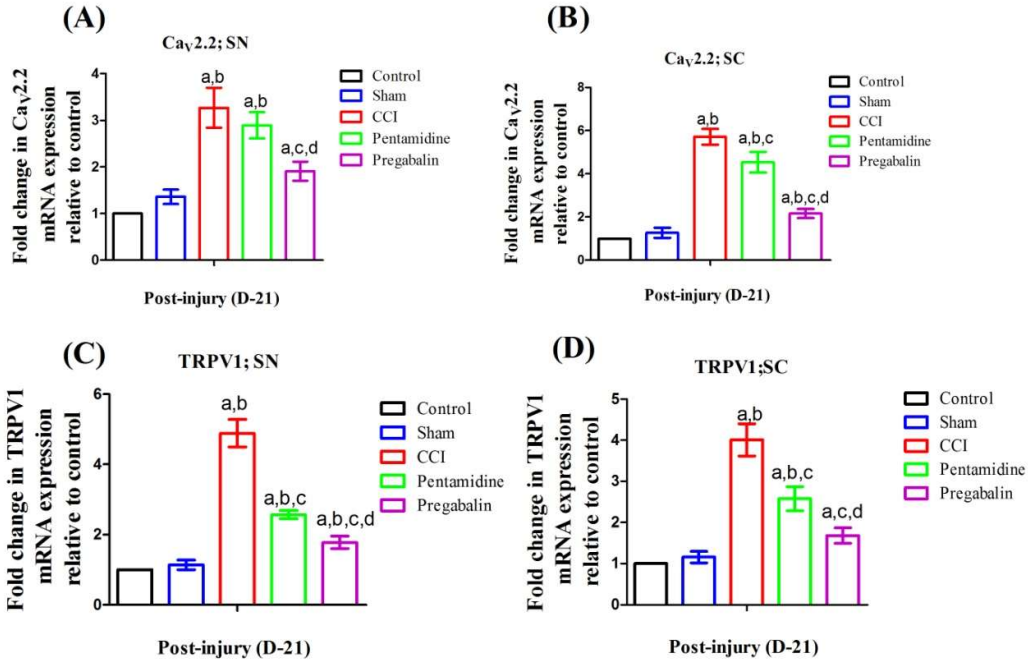

Figure 5.12: Effect of pentamidine on $Ca_V2.2$ and TRPV1 mRNA expression in the SN (A and C respectively) and SC (B and D respectively). All values are in mean ± SD (n=4 rats/ group). $^{a}p<0.05$, $^{b}p<0.05$, $^{c}p<0.05$, and $^{d}p<0.05$ compared to control, sham, CCI, and pentamidine respectively. (One-way ANOVA followed by Tukey's multiple comparison post-hoc test)

5.2.2.5. Effect of pentamidine on the expression of S100b in SN and SC

To further validate the effects of pentamidine on the S100b post-CCI in the SN and SC, we performed an immunofluorescence assay to observe the localization of S100b as illustrated in **Figures 5.13 and 5.14**. Our findings showed that there was increased fluorescence intensity in the CCI group. One-way ANOVA followed by post hoc test revealed a significant difference in fluorescence intensity of S100b expression among the groups in SN ([$F(4,14) = 16.84$; $p<0.05$]) and SC ([$F(4,14) = 22.48$; $p<0.05$]) compared to the control and sham group. Treatment with pentamidine and pregabalin significantly attenuated the CCI-induced increase in the fluorescence intensity of S100b. However, the effect produced by pentamidine was more prominent compared

to pregabalin. These observations are consistent with the clinical reports which showed an exaggerated response of S100b in traumatic brain injury (Lécuyer, Mercier et al. 2021). Further, S100 family proteins are reported to get activated upon binding with calcium and in the CCI model of NP, we observed elevated $(Ca^{2+})_i$ level in SN and SC. The activated S100 proteins tend to modulate glial cell activation, triggering inflammatory responses due to the release of pro-inflammatory cytokines and chemokines via NF- κB or calcium-dependent pathway, contributing to the chronic nature of NP (Michetti, Di Sante et al. 2021). Coherently, pharmacological blockade of S100b with pentamidine treatment in CCI rats mitigated NP phenotypes and also improved neuroinflammation as shown in **Figure 5.18**.

5.2.2.6. Effect of pentamidine on the CCI-induced microglial activation in SN and SC

The CCI-induced increase in the microglia activation was confirmed by immunofluorescence assay as depicted in **Figure 5.15**. The fluorescence intensity of Iba-1 (ionized calcium-binding adapter molecule 1) was used as a measure of microglial activation and DAPI was used for counterstaining the nucleus. Statistically, one-way ANOVA revealed that there was a significant difference in fluorescence intensity of Iba-1 expression in SC sections among the group ([$F(4,14) = 14.70$; $p<0.05$]**)**. The post hoc test demonstrated that Iba-1 intensity had significantly elevated in the CCI group compared to naïve rats that were almost abrogated by the pentamidine treatment ($p < 0.05$) on D-21. However, pregabalin-treated animals did not show any effect on CCI-induced increase in Iba-1. Notably, there were no significant differences between the control and sham group. Hence, our findings confirm that there was activation of microglia following CCI as suggested earlier (Nishihara, Tanaka et al. 2020). Besides,

previous studies have also reported that abnormal increase in S100b induces persistent microglial activation that is associated with the maintenance of hyperalgesia and allodynia (Hains and Waxman 2006) and also contributes to the complex pathophysiology of NP (Adami, Sorci et al. 2001). The injury-induced abnormal rise in S100b is reported to be detrimental to the neurons as well as the glial cells and via neuron-glial interactions; they amplify the release of pro-inflammatory cytokines contributing to the sensitization of the ascending pain pathways (Michetti, D'Ambrosi et al. 2019).

5.2.2.7. Effect of pentamidine on the CCI-induced astrocytes activation in SN and SC

The initiation of peripheral injury-induced NP is documented to be highly influenced by the neuroimmune alterations that activate resident immune cells of the nervous system (Hains and Waxman 2006). Therefore, the CCI-induced increase in the astrocyte activation in SN and SC was confirmed by immunofluoresence assay as depicted in **Figure 5.16 and 5.17** respectively. Statistically, one-way ANOVA revealed that there was a significant difference in fluorescence intensity of GFAP expression in SN and SC sections among the group ([$F(4,14) = 25.17$; $p<0.05$] and [$F(4,14) = 26.95$; $p<0.05$] respectively**)**. The post hoc test demonstrated that GFAP intensity had significantly elevated in the SN and SC of the CCI group compared to naïve rats. Treatment with pentamidine alleviated these alterations significantly ($p < 0.05$) on D-21 of the experimental protocol. However, pregabalin-treated animals did not show any significant effect on the CCI-induced increase in GFAP. Besides, in the SC, the GFAP-positive astrocytes of the naïve group exhibited round nuclei with a slender process while in the CCI group, they were swollen with hypertrophic appearance throughout

the section as shown in **Figure 5.17** which indicates the activated phenotype of astrocytes. So overall, our findings demonstrate that the glial cells are activated in this model of NP which was mitigated by a specific S100b inhibitor. Similar to our observation, research has demonstrated that inhibition of GFAP expression decreased NP phenotypes implying a possible and positive cause-and-effect connection between the astrocyte activation and chronic pain (Ji, Berta et al. 2013). Additionally, astrocytes are strongly associated with the preservation of the blood-brain barrier's integrity. Studies have shown that aberrant activation of the astrocytes may lead to a disruption in the selective permeability of the blood-brain barrier (Michinaga and Koyama 2019). Hence, our results clearly confirm that even though there is an injury caused to the peripheral nervous system in the CCI model of NP but neuroinflammation is also observed in the central nervous system i.e., SC.

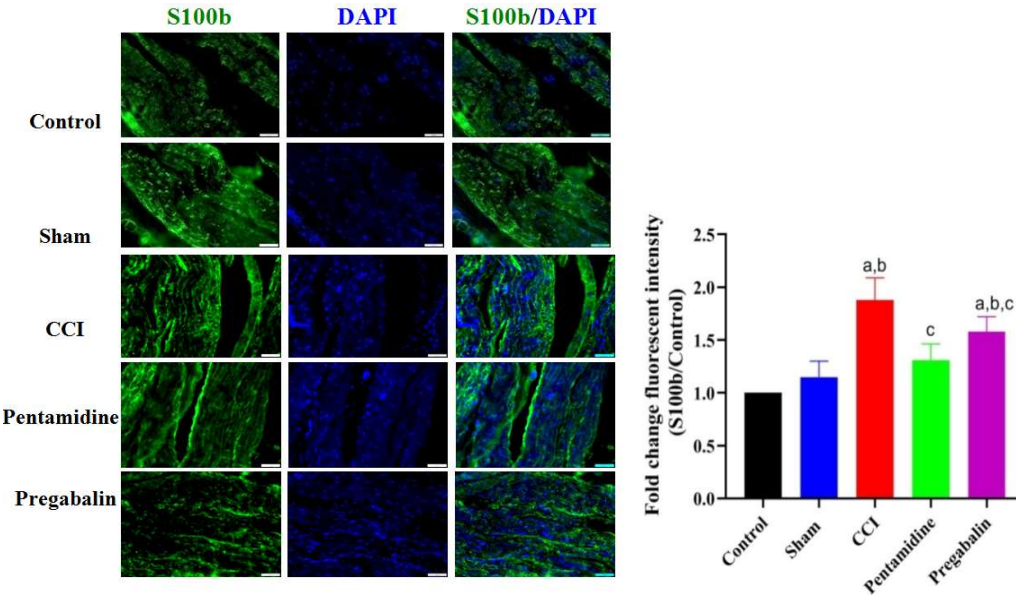

Figure 5.13: Effect of pentamidine on S100b expression in the SN. Scale bar was set at 50 µM with 20X magnification. All values are in mean ± SD (n=3 rats/ group). $^{a}p<0.05$, $^{b}p<0.05$, $^{c}p<0.05$, and $^{d}p<0.05$ compared to control, sham, CCI, and pentamidine respectively. (One-way ANOVA followed by Tukey's multiple comparison post-hoc test)

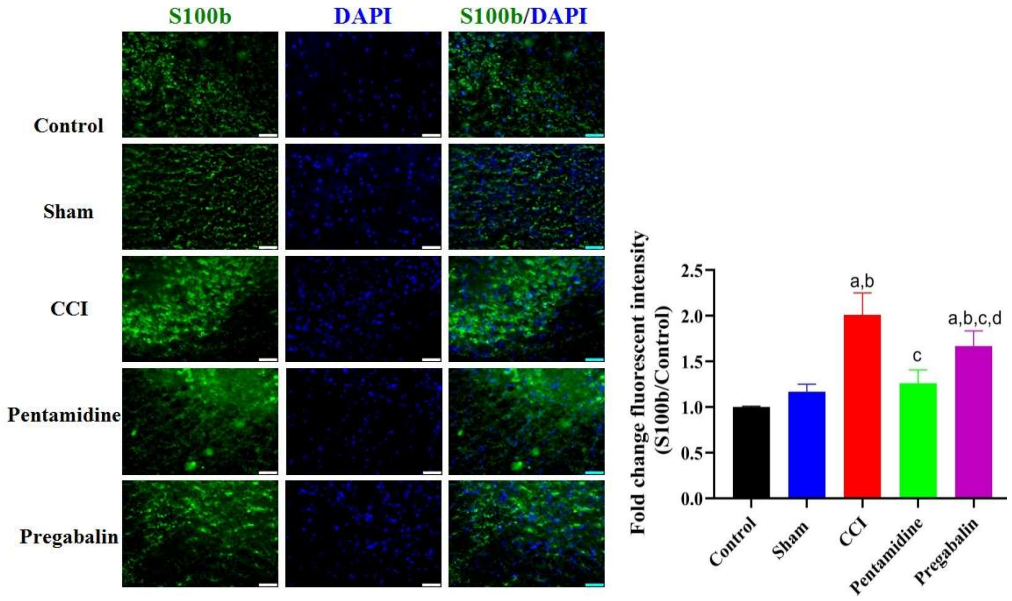

Figure 5.14: Effect of pentamidine on S100b expression in the SC. Scale bar was set at 50 µM with 20X magnification. All values are in mean ± SD (n=3 rats/ group). [a]p<0.05, [b]p<0.05, [c]p<0.05, and [d]p<0.05 compared to control, sham, CCI, and pentamidine respectively. (One-way ANOVA followed by Tukey's multiple comparison post-hoc test)

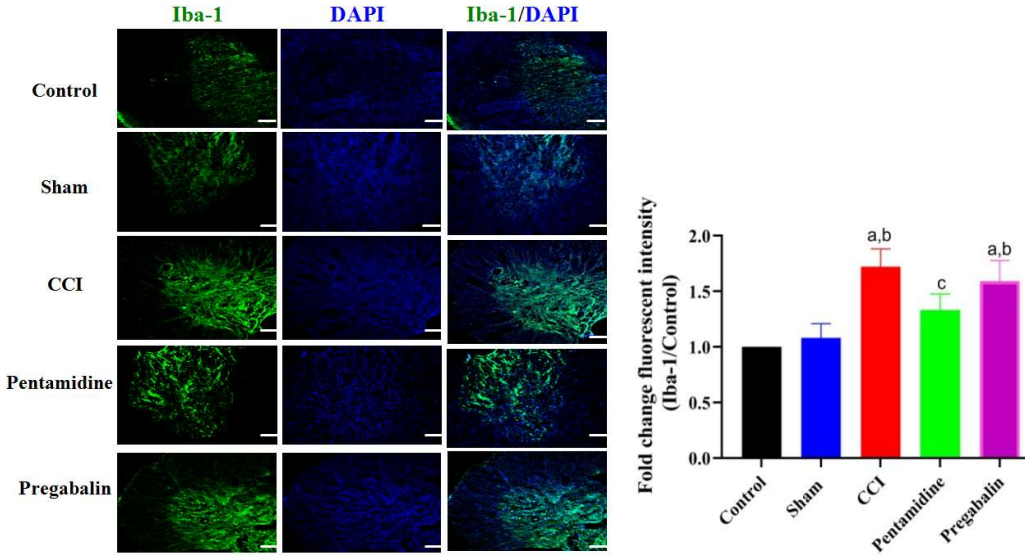

Figure 5.15: Effect of pentamidine on Iba-1 expression in the SC. Scale bar was set at 50 µM with 20X magnification. All values are in mean ± SD (n=3 rats/ group). [a]p<0.05, [b]p<0.05, and [c]p<0.05 compared to control, sham, and CCI respectively. (One-way ANOVA followed by Tukey's multiple comparison post-hoc test)

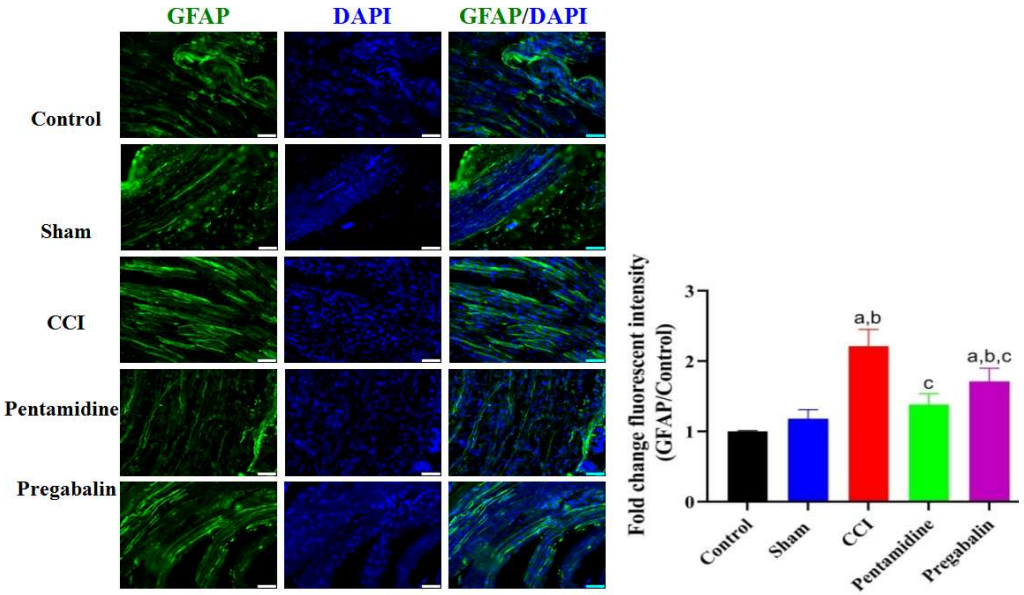

Figure 5.16: Effect of pentamidine on GFAP expression in the SN. Scale bar was set at 50 µM with 20X magnification. All values are in mean ± SD (n=3 rats/ group). $^{a}p<0.05$, $^{b}p<0.05$, and $^{c}p<0.05$ compared to control, sham, and CCI respectively. (One-way ANOVA followed by Tukey's multiple comparison post-hoc test)

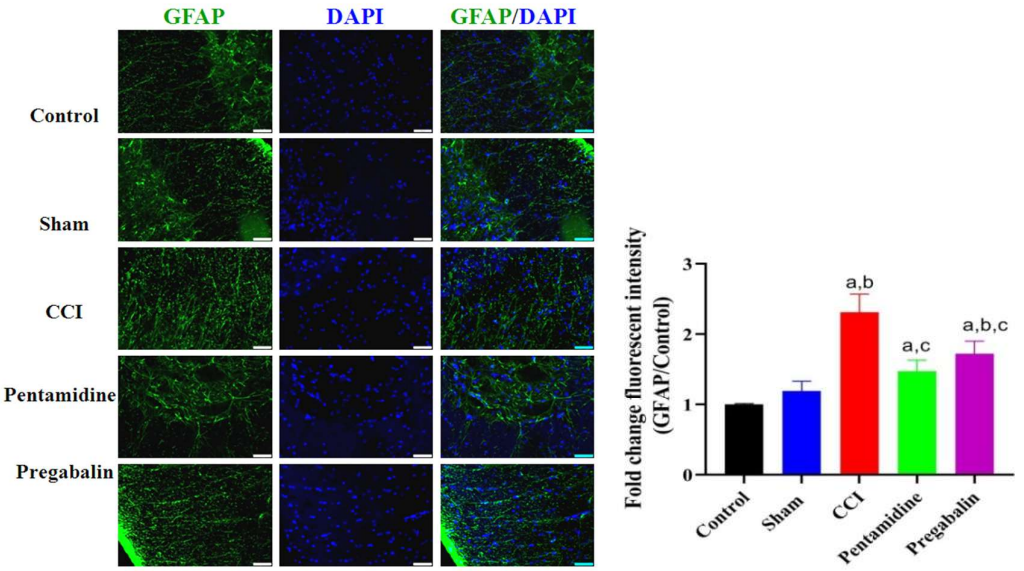

Figure 5.17: Effect of pentamidine on GFAP expression in the SC. Scale bar was set at 50 µM with 20X magnification. All values are in mean ± SD (n=3 rats/ group). $^{a}p<0.05$, $^{b}p<0.05$, and $^{c}p<0.05$ compared to control, sham, and CCI respectively. (One-way ANOVA followed by Tukey's multiple comparison post-hoc test)

5.2.2.8. Effect of pentamidine on the CCI-induced neuroinflammation

The CCI-induced increase in the pro-inflammatory cytokines was measured in the SN and SC of the rats expressing NP phenotypes as represented in **Figure 5.18**. The objective was to investigate the downstream pro-inflammatory cytokines that are produced after the activation of S100b and whether specific S100b inhibitors can alleviate NP via mitigation of neuroinflammation. In our study, the mRNA gene expression of NF-κB was performed and significant differences were observed among different groups. One-way ANOVA revealed significant variations in NF-κB gene expression in SN and SC ([F (4, 19) = 49.49; $p < 0.05$] and [F (4, 19) = 39.48; $p < 0.05$] respectively) (**Figure 5.18i and ii**). The post hoc test demonstrated that NF-κB mRNA expression had significantly elevated in the SN and SC of the CCI group compared to naïve and sham rats. Specifically, there was a 2.48 and 2.06-fold increase in NF-κB expression in SN and SC of CCI rats respectively. However, the treatment with pentamidine alleviated the increase in NF-κB significantly ($p < 0.05$), a key regulator of inflammatory responses on D-21.

Further, statistically, one-way ANOVA also revealed that there was a significant difference in TNF-α level in the SN and SC among the group ([F(4,19) = 154.8; $p<0.05$] and [F(4,19) = 136.2; $p<0.05$] respectively**)** as depicted in **Figure 5.18ii A and C**. Similarly, we observed significant differences in pro-inflammatory cytokine i.e., IL-6 among the various groups in SN and SC ([F(4,19) = 37.91; $p<0.05$] and [F(4,19) = 52.68; $p<0.05$] respectively**)** as shown in **Figure 5.18ii B and D**. The post hoc test demonstrated that TNF-α and IL-6 levels was significantly elevated in CCI group compared to naïve that was reversed following pentamidine treatment ($p < 0.05$). Likewise, in support of our observation, previous reports have demonstrated S100b-

mediated NF-κB pathway activation that led to downstream pro-inflammatory cascade activation (Barros, Barateiro et al. 2022).

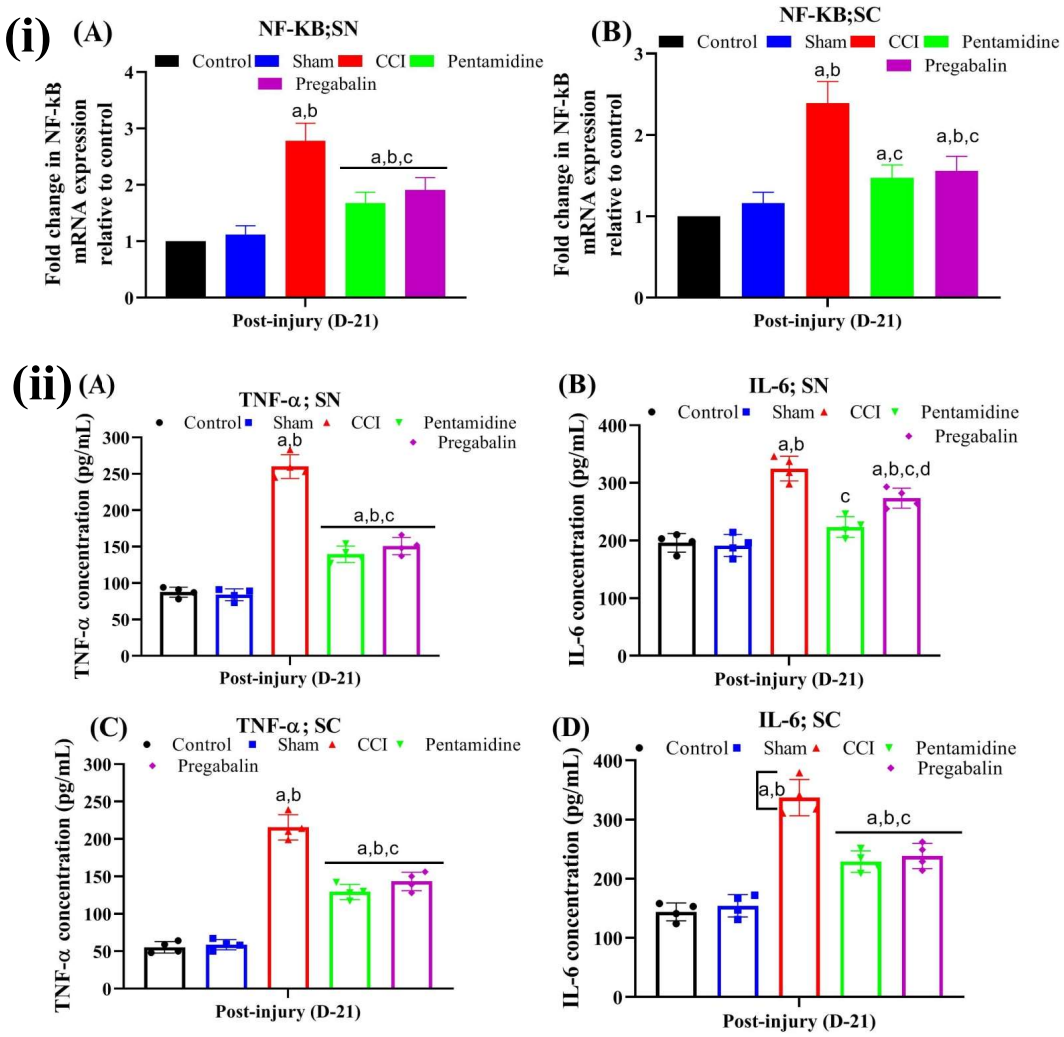

Figure 5.18: Effect of pentamidine on (i) NF- κB mRNA expression and (ii) TNF-α and IL-6 levels in the SN and SC. All values are in mean ± SD (n=4 rats/ group). $^{a}p<0.05$, $^{b}p<0.05$, $^{c}p<0.05$, and $^{d}p<0.05$ compared to control, sham, CCI, and pentamidine respectively. (One-way ANOVA followed by Tukey's multiple comparison post-hoc test)

5.2.2.9. Effect of pentamidine on the neuronal morphology post-CCI injury

We analyzed the neuronal morphology in the SC sections post-CCI injury as shown in **Figure 5.19**. In the CCI rats, there was disintegration and retraction of the dendrites of

neurons present in the SC. The dendrites were broken into small fragments and there was also a reduction in the number of branching across the soma following injury to the peripheral nerve. However, treatment with pentamidine as well as pregabalin led to dendrite arborization. Further, we traced individual neurons that were subjected to Sholl analysis as represented in **Figure 5.20i**. The results showed that the intersections of dendrites with concentric circles at each radius were dramatically decreased in the injured rats. Statistical analysis using the one-way ANOVA approach demonstrated significant differences in the total length of the dendrites [$F(4, 19) = 12.29$, $p < 0.05$, **Figure 5.20iiC**] among different experimental groups. Post-hoc analysis revealed that following treatment with pentamidine significantly increased the total length of the dendrites compared to the CCI group which had decreased significantly post-injury to the nerve. Furthermore, the dendritic arbors in the treatment group were longer and had more intersections at each radius compared with those in the CCI group, as determined by Sholl analysis (**Figure 5.20iiA and B**). These results indicate that spinal neuronal dendrite arborization degenerated dramatically after CCI, but the degeneration was alleviated upon specific inhibition of S100b. Similarly to our observations, it has been reported that when synaptic rewiring occurs, the remaining neurons try to rewire to make newer synaptic neural connections in order to repair and compensate for the loss of function (Tan, Stamboulian et al. 2008). The extent of functional recovery post-injury depends on the efficiency of neural circuit reconnection such as reactivating and reorganizing the intraspinal neuronal connections.

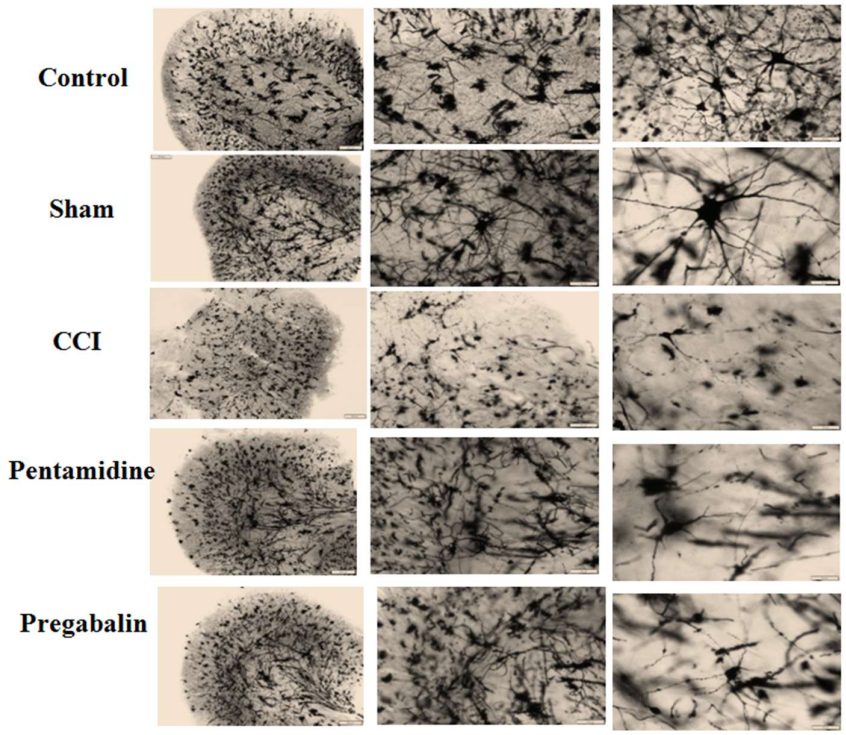

Figure 5.19: Representative images of Golgi-cox impregnated spinal cord slice of control, sham, CCI, pentamidine, and pregabalin treated rats. Scale bar was set at 200, 100, and 50 µM with 4, 10, 20X magnification.

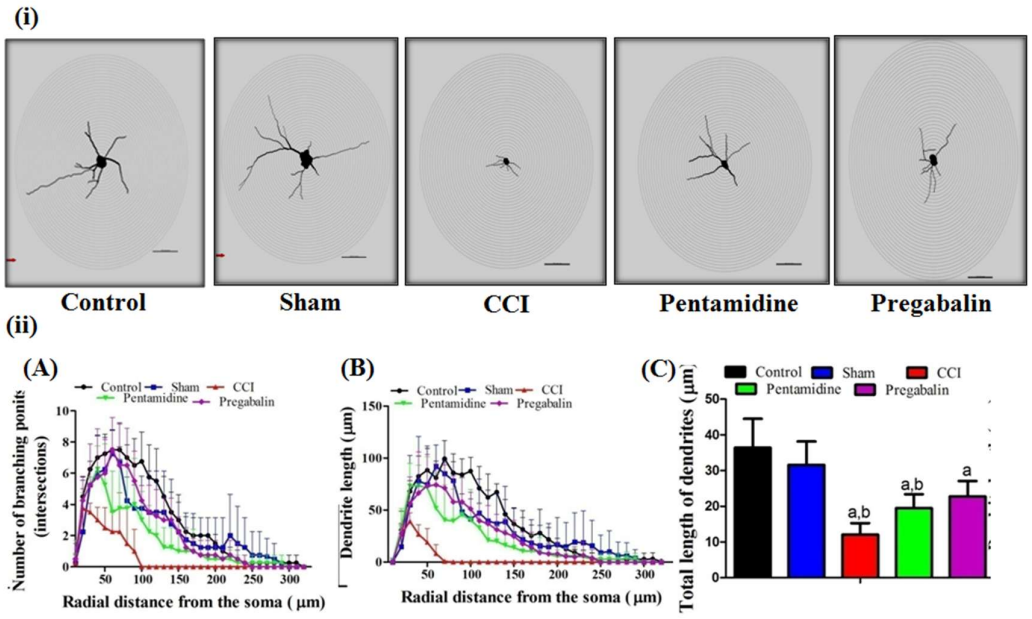

Figure 5.20: (i) Representative image of the camera lucida drawing of neuron of SC which is superimposed over concentric circles using Sholl analysis. (ii) Effect of pentamidine on (A) number of branching points across the soma, (B) dendrite length at radial distance from the soma and (C) the total length of dendrites. All values are in

mean ± SD (n=4 / group). [a]p<0.05 and [b]p<0.05 compared to control and sham respectively. (One-way ANOVA followed by Tukey's multiple comparison post-hoc test)

5.2.2.10. Effect of pentamidine on the CCI-induced changes in NF-L expression in the SN

Neurofilament (NF) proteins are the crucial components of the cytoskeleton in the neurons of nervous systems and they serve as the structural framework for axons (Huehnchen, Schinke et al. 2022). In the context of NP, the negative symptoms are often reported to be correlated with the deterioration of bigger myelinated axons, whereas positive and pain symptoms are typically connected to the impairment of smaller unmyelinated fibers (Scripture, Figg et al. 2006). Therefore, in the present study, we evaluated the effect of CCI on NF-L and observed that there was a significant decrease in the fluorescent intensity of NF-L in the rats after the injury. One-way ANOVA followed by a post-hoc test demonstrated significant changes among the group [$F(4,14) = 35.34$; $p<0.05$]. In the control group, the alignment of NF-L is observed but in the CCI rats, NF-L is found to be fragmented and scrambled as illustrated in **Figure 5.21**. Treatment with pentamidine rats exhibited elevated NF-L expression in the SN compared to the CCI group, indicative of axonal regrowth. However, the pregabalin treatment was found to be not as effective as a specific S100b inhibitor. Our data agree with previous preclinical work where axonal damage elevated S100b levels that contributed to a pro-inflammatory environment and decreased the NF level in the axon (Kuhle, Gaiottino et al. 2015, Adamczyk, Morawiec et al. 2023). Therefore, these results ascertain that modulating S100b has the axonal repairing potential and thus the functional repair was observed during the pain behavioral assessment tests (**Figure 5.9**).

5.2.2.11. Effect of pentamidine on the gastrocnemius muscle post-CCI injury

Post-CCI injury, there was a significant reduction in the weight of gastrocnemius muscle of the ipsilateral side of CCI rats (i.e., 0.462 ± 0.064187 g) compared to the control rats i.e., 1.48 ± 0.070214 suggesting muscle atrophy (**Figure 5.22**). One-way ANOVA revealed significant variations in the muscle weight among groups ([F (4, 24) = 280.5; $p < 0.05$] (**Figure 5.22C**). Tukey's post hoc test demonstrated that following the constriction injury to SN, the weight of gastrocnemius muscle had reduced significantly in the CCI group compared to naïve and sham rats which was reversed following pentamidine treatment ($p < 0.05$). The gastrocnemius muscle is the largest muscle which is innervated by the branches of the SN and helps in the flexion of the knee, aiding in body movement. However, denervated muscles lose signal transmission from the nervous system and are unable to maintain the contraction function. Thus, injury to the SN is reported to cause immobilization or reduced use of the affected limb (Choe, Kim et al. 2011). Prolonged disuse or restricted movement of the affected limb subsequently causes muscle atrophy as reported preclinically (Choe, Kim et al. 2011) and this is consistent in patients suffering from NP (Bhindi, Angliss et al. 2022). Further, there are reports of reduced muscular protein synthesis and an increase in protein breakdown, causing myatrophy and reduced gastrocnemius muscle weight (Wang, Chen et al. 2021) as observed in our study **Figure 5.22A**. Moreover, the histological analyses of the gastrocnemius muscle of control rats revealed homogeneous morphology with the densely packed polygonal-shaped skeletal muscle fibres along with the peripheral oval nuclei. On the other hand, the CCI group exhibited fragmentation of the sarcoplasm with mononuclear cell infiltration (**Figure 5.22B)**. There was also a widening of endomysium observed in the injured rats. However,

treatment with pentamidine significantly increased the gastrocnemius muscle fiber cross-section area to 49.6 ± 3.51 from 37.8 ± 3.89 % as observed in CCI rats. In light of these findings, it can be inferred that motor impairments are closely linked to the CCI model of NP and specific S100b inhibitor reversed all core symptoms of NP along with the observed motor incoordination.

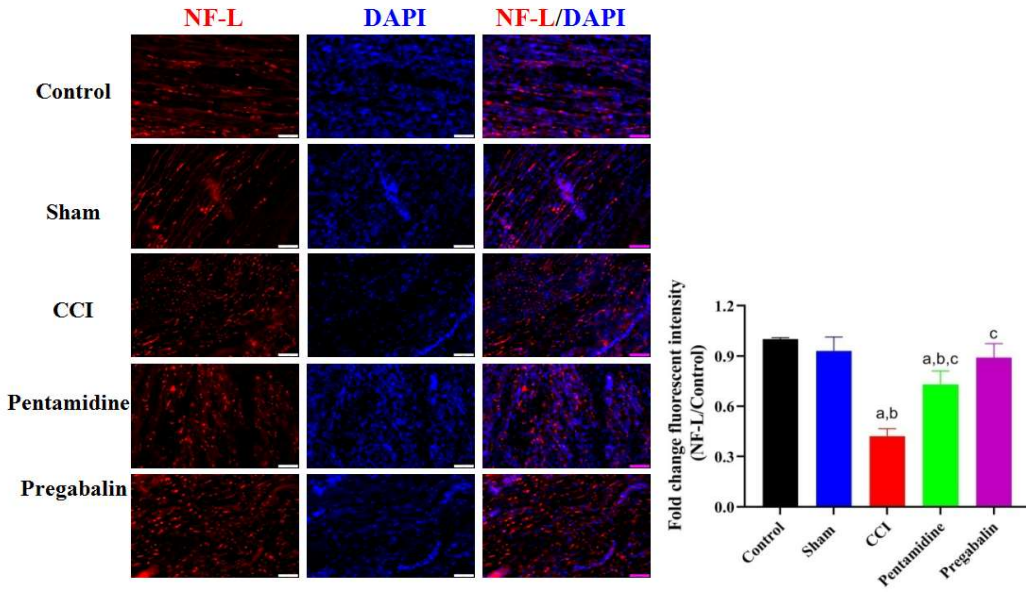

Figure 5.21: Effect of pentamidine on NF-L expression in the SN. Scale bar was set at 50 µM with 20X magnification. All values are in mean ± SD (n=3 rats/ group). $^{a}p<0.05$, $^{b}p<0.05$, and $^{c}p<0.05$ compared to control, sham, and CCI respectively. (One-way ANOVA followed by Tukey's post-hoc test)

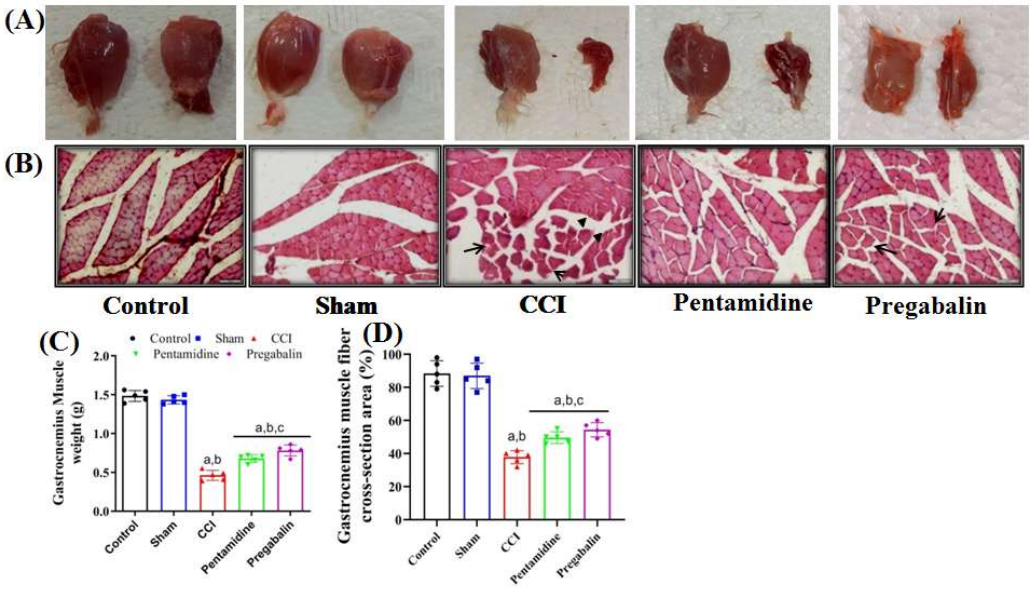

Figure 5.22: (A) Representative images of the gastrocnemius muscle of the contralateral and ipsilateral side of the leg. (B) Representative image of the histological analyses of gastrocnemius muscle stained with hematoxylin and eosin at the end of 21st day post-surgery. (C and D) The effect of pentamidine on gastrocnemius muscle weight and cross-section area of muscle fibers. All values are in mean ± SD (n=5 rats/ group). $^{a}p<0.05$, $^{b}p<0.05$, $^{c}p<0.05$, and $^{d}p<0.05$ compared to control, sham, CCI, and pentamidine respectively. (One-way ANOVA followed by Tukey's multiple comparison post-hoc test)

5.3. Conclusion

In the current study, our findings establish the temporal dynamics and significant details about the involvement of intracellular calcium and S100b protein levels in the progression and sustenance of CCI-induced NP in rats. Following CCI, there was a notable time-dependent increase in the intracellular calcium and S100b protein level in both the SN and SC acutely 1 h post-injury. However, treatment with a specific S100b inhibitor i.e., pentamidine significantly reversed the NP phenotypes induced by CCI, suggesting that S100b plays a pivotal role in the pathophysiology of NP. Pentamidine treatment also demonstrated efficacy in alleviating motor deficits associated with the CCI model. Notably, the study also demonstrated hyperactivation of astrocytes and microglia induced by S100b which was reduced following the pentamidine

administration. Therefore, by inhibiting glial cell activation, pentamidine disrupted the feed-forward loop of inflammation and pain, contributing to the reversal of NP phenotypes. Moreover, pentamidine treatment significantly lowered the S100b-induced increase in pro-inflammatory markers, specifically TNF-α and IL-6, in SC and SN post-injury. However, unlike pregabalin, pentamidine was unable to reverse the elevated intracellular calcium levels in the SN and SC post-injury. In conclusion, these findings provide compelling evidence supporting the role of S100b in the pathogenesis of NP and highlight the therapeutic potential of S100b inhibition.

Summary

- There is temporal increase in the intracellular calcium and S100b level in SN and SC post-CCI.
- Treatment with specific S100b inhibitor i.e., pentamidine significantly reversed the NP phenotypes.
- The motor deficits due to CCI were also alleviated following pentamidine treatment.
- Pentamidine lowered the S100b-induced increase in pro-inflammatory markers (TNF-α and IL-6) in SC and SN post-injury to the peripheral nerve.
- Pentamidine also reduced the S100b-induced hyperactivation of astrocytes and microglia.
- Unlike pregabalin, pentamidine was unable to reverse the elevated intracellular calcium level in the SN and SC post injury to the peripheral nervous system.

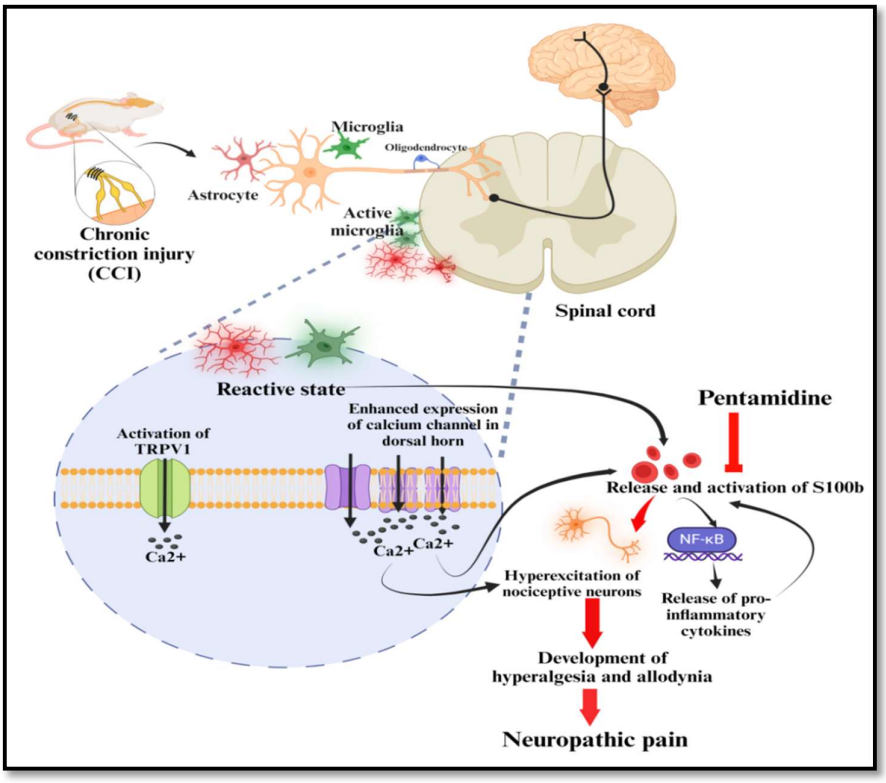

Figure 5.23 showcases the specific objective's outcome in exploring the molecular mechanism behind neuropathic pain (NP) in a CCI-induced rat NP model. It suggests that the development and progression of NP is associated temporal increase in the intracellular calcium and calcium-binding protein i.e., S100b. Treatment with pentamidine, a specific S100B inhibitor, significantly reversed the neuropathic pain phenotypes induced by CCI. Besides, CCI of peripheral nerve caused hyperactivation of astrocytes and microglia that was induced by S100B and pentamidine attenuated these observed changes. Treatment with pentamidine also lowered the S100B-induced increase in pro-inflammatory markers, specifically TNF-α and IL-6, in both the SC and SN post-injury. Therefore, these findings highlight that S100b is involved in progression and development of NP phenotypes in the CCI-induced NP model and could be the essential factor for an analgesic drug for better management of NP.